Interactive comment on "Joint Analysis of Convective Structure from the APR-2 Precipitation Radar and the DAWN Doppler Wind Lidar During the 2017 Convective Processes Experiment (CPEX)" *by* F. Joseph Turk et al.

Anonymous Referee #1

Received and published: 17 April 2020

The paper presents some very interesting measurements collected during the CPEX experiment by joint Doppler Aerosol Wind Lidar and dual frequency Doppler radar observations. The paper is very important because lays the foundation on how to integrate these two different Doppler observing systems. The paper is generally very well written. I am looking forward seeing the data used for a better understanding of the linking between 3-D air motion and cloud structure in a peer-reviewed journal.

I have mainly some comments to improve the layout and to add the information content of some of the figures. Also, Sect 4 could be improved.

Line 140: "any developed" ==> developed

Fixed.

Fig.4: it is very difficult to read this figure. In particular the overlapping of the image colour and the coloured dots is particularly troublesome. Why not shifting the dots upwards by 0.5 degree latitude (properly commenting on that in the caption) ?

We agree, in fact since Fig 5 is the figure that is supposed to represent the DAWN LOS sampling, we just removed these dots from this figure and the color scales represents the Ku and Ka-band reflectivity. In Figures 6 and 7, which zooms in to the various LOS profiles, the second colorbar for the lowest level is reinstated.

Fig5: Maybe it is worth saying that no image colour is present if no clouds with reflectivity above radar sensitivity are present in the layer.

We have added this (no image color= no clouds present that are above the APR-2 radar sensitivity).

Fig7: colour-scale is in dBZ not dB, right? (also line 223 and through the document)

Yes, that's correct. We have fixed this terminology throughout.

Fig8: red box: If the red box represents the blind zone it should follow the aircraft flight level and go oblique before scan 500. "above 6-km (where the SNR is highest), and below 3-km (where the aerosol content is higher)" it is a little bit misleading because I think in both cases the SNR is high, in the first case because of the shorter range, in the second for the higher backscattering. In general, it is not clear to me why between 1000 and 1500 (there is not a clear range dependence in the upper part, is the lower part structure related to aerosol in the first two km?) the black dots are distributed like they are. Maybe over-plotting lidar SNR contour levels could help. Same applies to Fig.10-12-14. Also isn't in all such figures a lost opportunity? Why not showing for some of the black dots the wind direction? We could actually appreciate wind shear in proximity of convective clouds.

One reason for the "lower part structure" referred to is likely due to clouds that may be present, but below the APR-2 detectability, so we have no "proof" that they are really there. Some of these clouds are "thin" enough that DAWN can penetrate and still have sufficient dynamic range (see the reply to the comment below with an example figure of

this situation), others penetrate only partially. Or some profiles occurred during slightly different aerosol concentration in the lower 1-2 km than did other nearby profiles.

The 2-km and 8-km wind barbs are plotted on Figure 4, which corresponds with Figure 7. In other words the flight segment shown in Figure 4 maps one-to-one with the x-axis on Figure 7. If I add anything more to Figure 7, it will clutter it up.

But your comment is a very good one which gave me an idea to present the wind hodographs for each of the four one-hour time segments. From these, the directional wind shear (if present) is more obvious. These are now included in the paper. I did this for the 2-vs-8 km levels and the 2-vs-6 km levels (Figure 7, similarly for other segments). Which show very interesting shear, especially in the 1830-1930 period. Furthermore, I separated the hodographs into quadrants (NE, SE, SW, NW) relative to the approximate center (25.2N 73W) of the flight box on this date. This shows the sustained 2-8 km shear in the area SW of the area of interest, that flips sign by about 90-deg when compared to the 2-6 km shear.

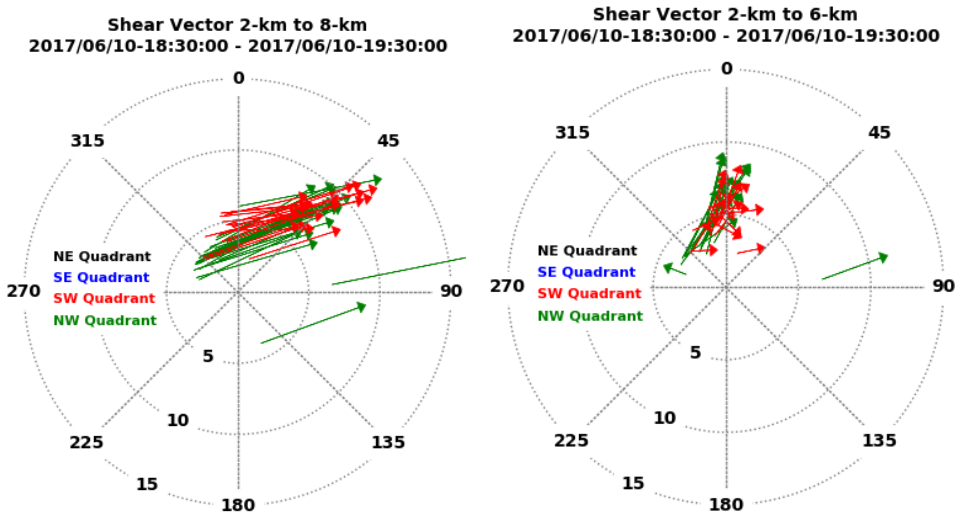

Fig.8: about the "continuous "impenetrable" cloud structures" comment obviously the lidar will see through the 3D structure, no question. I am a little bit skeptical about the profile at 192746 UTC; I cannot imagine that the lidar signals goes through the black dots as currently drawn; are we guessing here that there is basically no cloud liquid for that specific path and light will go through rain and ice? otherwise couldn't we argue that the path maybe a little bit different from the one currently drawn (you have pointing uncertainties to account for, haven't you?)?

The black dots in Figure 8 (in the revised paper) indicate the DAWN (u,v) *wind profile* vertical locations. The wind profile in turn is created by merging all five LOS beams, each with a different relative viewing direction. These are combined in an optimal way (the ASIA processing referred to in Section 2), and the resulting vertical profile is "placed" at the geographical centroid location from all five beams. Owing to the DAWN conically-located LOS locations, the "location" of the final profile is somewhat arbitrary, but if there are two beams each on either side of the DC-8 flight track, then this location will be somewhere along the aircraft subtrack, but not directly under the DC-8. It represents an aggregation or combination of five different views from different angles, so it really represents some sort of average wind from the air sampled collectively from all five beams. In other words, bin-by-bin comparisons with the APR-2 nadir reflectivity as in Figures 8 needs to take the instrument scan characteristics into account. We have added wording to this effect in the discussion of Figure 8 and the others similar to it.

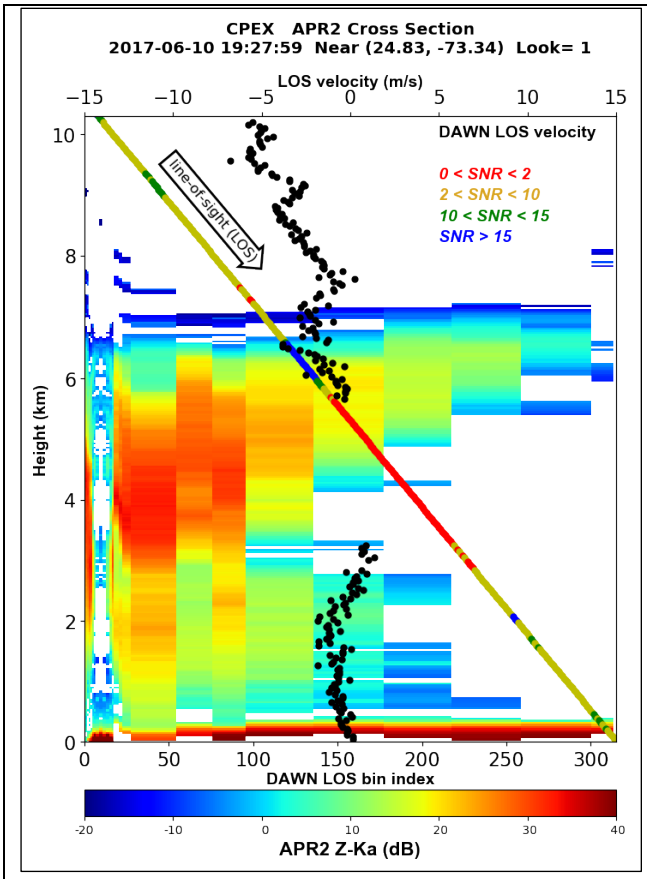

As for the question on DAWN penetration through clouds. This is something that applies to each of the LOS beams. The radar and lidar systems scan and "stare" very differently. Each DAWN LOS profile is pointed off-nadir 30 degrees at different azimuth angles (Figure 1), where is "stares" over a longer integration time than the APR2 radar (APR2 collects 24 rays as it scans across track in about 1.2 seconds). So, indeed you are absolutely right that DAWN LOS and APR-2 beam matching has bin/beam matching uncertainties associated with it. We did not show this in the manuscript. When each DAWN LOS bin (about 30-m) is mapped to APR2, you end up with a very coarse interpolation. See the figure to the left, which I did not include in the manuscript. Here you can envision the DAWN LOS beam (LOS bin index 1 is the first bin below the DC-8 and bin 320 is the bin at the surface) like a pencil pointing through the APR-2 scanning "volume" covered by its cross-track swath as the DC-8 moves forward. Now imagine the APR-2 cross section along this LOS cross section. Notice how many APR-2 beams are "replicated" (no interpolation was done) owing to the different scan modes of the two instruments. In this case, this LOS beam penetrated an upper cloud portion between 7- and 4-km height, that was sufficiently optically thin enough that DAWN could penetrate it (SNR fell to below 2), but still had dynamic range to capture winds below it (SNR was near 10 near the surface). But, another of the other four LOS beams (of the five total) was unable to penetrate to the near-surface (example not shown). This would be reflected in the quality of the ASIA wind profile processing when it had only four LOS beams to work with. If there were even more cloudy conditions, even less LOS beams are available to retrieve the wind profile. Nonetheless, this picture gives an example of where (in the vertical) the cloud layers are, and how far DAWN could penetrate though the cloud before losing its signal for good.

Sect.4: I understand that the retrieval of wind must be done in the aircraft reference frame for the interpretation it is much better to go back to the usual system (E-W and N-S winds). Since the DC-8 heading is known this is a simple conversion. By so doing you will get rid of all the discussion about the heading and we will actually see the "real winds" (which are the relevant ones for the study of "dynamical processes"). Also the u,v notation is confusing since it is typically used for E-W and N-S winds.

Exactly right. For this example, we intentionally chose the June 11 case since the DC-8 flight bearings were (fortuitously) along E-W and N-S (or vice versa) directions, so this conversion was not necessary. We changed the notation as suggested in the text and Figure 20 (in the revised manuscript). But in general, yes, the aircraft cross-track winds are some mixture of u and v, so the DAWN winds could be transformed (rotated at each level) into the aircraft frame of reference. We think that this June 11 case made the DAWN-APR2 cross-track wind comparison easier to understand.

Interactive comment on "Joint Analysis of Convective Structure from the APR-2 Precipitation Radar and the DAWN Doppler Wind Lidar During the 2017 Convective Processes Experiment (CPEX)" *by* F. Joseph Turk et al.

Anonymous Referee #2

Received and published: 22 April 2020

General comments

This well written manuscript presents novel, unique and relevant collocated airborne Doppler lidar and radar measurements in complex, convective subtropical environments. Focus is set to a common display of both instruments' data sets from two exemplary NASA DC-8 research flights, to show regions of common data overlap and the measurement limits of each instrument. The paper is fully suitable to the scope of AMT, and both the scientific relevance and the data quality are outstanding. However, or because of this, I find it disappointing that scientific conclusions from such an interesting instrument combination are missing, and that the reader is just referred to future studies.

There exists a WCRP Grand Challenge on Clouds, Circulation and Climate Sensitivity (which the authors do not address - anyway), because one of the big science questions is the feedback of convection on dynamics. This DC-8 instrumentation is perfectly suited to address this question, and I think the readers would like to see more details and (preliminary) conclusions hereto.

This manuscript is intentionally weighted almost totally to the observational aspects. As mentioned in the introduction (…*this manuscript will describe and present only the airborne precipitation radar and DWL observations; a separate manuscript will present the associated mesoscale model simulations and DWL data assimilation experiment results*) and in the last paragraph in the conclusions (….*this manuscript provides the observational context for a separate mesoscale model data assimilation study, which is aimed at quantifying the impact of the DAWN measurements on the analyzed atmospheric state variables and on the forecasted precipitation when the DAWN wind profile observations were assimilated into the model*), it is an introductory paper. A Part 2 paper that uses these CPEX data in a data assimilation (DA) study is forthcoming. If the field observations material and the DA study material was submitted as one manuscript, it would be a huge un-focused manuscript. Secondly, there is a technical audience that is mainly interested in the instrumentation and measurement aspects. This paper provides the details for that audience. On the other side of the coin, there is also a large DA community for wind vector DA (evidenced by the increasing number of Aeolus-related papers and presentations), but who already know the basic tenets of Doppler wind lidar and don't necessarily want to know about the CPEX campaign specifics, radar, etc. The second paper will align with that audience. The *Zhang et. al.* (2019) reference provides some indication of what will be in this second paper.

That all said, your comment is a good one and we did add some science related discussion to bridge these two manuscripts. We have mentioned some of our findings from the DA study during the discussion. We added new shear figures that depict the wind shear between the 2- and 8-km and 2- and 6-km levels, which highlight the importance of when and where winds are sampled. In our DA study, we believe that the timing and location of the DAWN observations during the first one-hour period (1830-1930 UTC) captured the wind shear between various mid-upper levels that was not as well defined in the control run, and that its assimilation led to the formation of more convergence and a precipitation pattern that agreed with where APR-2 noted the precipitation. These findings, if substantiated, may be relevant to the WCRP Grand Challenge mentioned, from an observational standpoint. From

space, a missing link has been the dynamical aspects. Space based instruments like GPM, and the various passive MW sounders (ATMS, etc.) measure "snapshots" of the condensed water field at some stage in the cloud/convection process, not their motion. We have tried to emphasize the connection between the air motion and the storm development. Capturing motion of air parcels (via a space based lidar) and how they tie into boundary layer processes is indeed a grand challenge.

So here is my suggestion how to avoid disappointment without too much extra effort. The interesting questions are: what is the evolution in time of the probed cloud cluster? Did you observe secondary circulations due to cloud growth? Is convergence or divergence visible in the measurements? So, at the end of section 3, maybe also 4, you should answer these questions. An extra, perhaps 3-d, sketch of the cloud cluster with the essential wind arrows resulting from all flight segments at both 2- and 8-km heights would be very helpful.

Very good suggestion, especially on the last point. Based on your comment and one from a different reviewer, we created 2-level wind hodographs for each of the four one-hour time segments. From these, the directional wind shear (if present, or how it evolves) is more obvious. We did this for the 2-vs-6 km levels and the 2-vs-8 km levels at each of the four one-hour time segments, to capture evolution. Furthermore, I separated this into quadrants relative to the approximate center of this flight box (25.2N 73W). Which show very interesting shear particularly in the 1830-1930 period. During this time there is sustained directional 2-vs-8 km wind shear west of the AOI, oriented from west to east. A similar analysis for the shear between 2-km and 6-km shows the shear oriented more south to north. Data gathered in the two hours after this (2030-2130) (Figure 14 in the revised paper) show that the 2-vs-8 km shear oriented itself more towards the southeast.

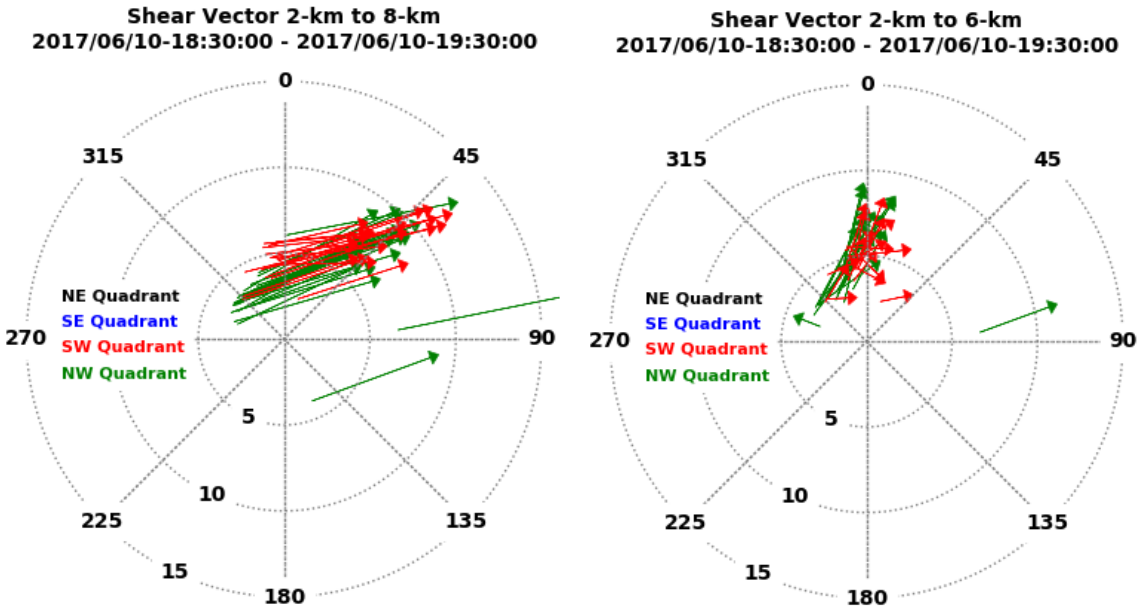

On the question of secondary circulations and convergence: From the scale of these observations alone, we can't readily pick out convergence since that requires a larger area and more spatially "complete" field than what these repeat pass, narrow swath DAWN data can provide, especially near the surface. We can say here that the assimilation of the DAWN winds (the Part 2 paper, not yet submitted) which used WRF-like mesoscale model simulations, showed a very discernable impact to wind and precipitation, enhanced surface convergence was noted when DAWN winds were assimilated, as well a more pronounced cold pool, as reflected in the precipitation location and timing.

Specific comments

The abstract is misleading. It repeats the nicely written overarching science issues from the introduction (it is OK to address them in the introduction), suggesting to the reader that these big questions are the main topic (which is not quite correct), but in fact it lacks the major results of the paper (= the answers to my above questions). Furthermore, it mentions "transport of water vapor" (line 15) and "Frequent dropsonde data" (l. 19) which both are not major topics of the paper.

Point well taken. We have revised the abstract accordingly.

Lines 37 and 64: these sentences highlight the importance of the vertical distribution of water vapor, a very interesting topic, yet which is (unfortunately) not addressed in this paper. The dropsondes could provide the humidity profiles, but I guess there were too few of them on these two flights to make solid statements, and/or this topic is beyond the scope of this study? Could you comment on this?

Good point. DAWN operates in a spectral band that is away from water vapor absorption. Actually, there is a follow-on CPEX campaign planned (in 2021) that will have, in addition to DAWN and APR-2, a water vapor lidar. From these joint observations, one will be able to depict high resolution water vapor structure together with its dynamical aspects. For this manuscript, we removed the dropsondes discussion since we did not analyze them, and there are many fewer of these compared to DAWN winds (the dropsondes provided important cal-val for the DAWN wind processing).

Line 79: ". . .radar and DWL observations from two exemplary flight days" to be more precise. In this context, I find that Table 1 is not at all needed.

Another purpose of this paper is to document the CPEX field campaign not only for the two dates/cases studied here, but also for future studies by others who may use this paper to pick out other dates that may be more relevant to their particular needs. We feel that Table 1 is important for this purpose.

Fig 1 is difficult to understand. Fig 5 suggests that at 2 km asl the +-45° lidar positions at 30° off-nadir angle have about the same separation than the APR swath width at +-25°. Could that be illustrated in Fig 1?

This figure is designed as a depiction rather than anything angularly or spatially accurate or to scale. A better depiction of the DAWN scanning is in the reference given (*Kavaya et al* 2014). What you say though is approximately correct: The spacing between the ground "footprints" of the DAWN beams at +/-45 degrees is about the same distance (8-km) as the APR-2 radar swath (given a 10-km DC-8 flight altitude). We have made reference to this in the Figure 1 caption.

Line 125: please explain the synoptic situation, and in more detail why you chose this particular situation out of 16 flights. Is the isolated cloud cluster you probed a beginning MCS? What is its relation to the extended cloud band to the north? Was this situation typical for the whole campaign, or was it a very particular "golden day"?

We have added some wording as to why this June 10 date was chosen for analysis. There are three key reasons: (a) This was an isolated, developing set of convective cells, isolated to some degree from large scale forcing effects, (b) the aircraft arrived on-station with sufficient time to make several "box-like" and "crossover" patterns to sample the air mass from different locations, in a developing/growth phase, (c) upon arrival, the clouds during this time were not sufficiently vertically developed and the DC-8 pilot was able to pass over the tops of nearly all clouds during the available on-station time.

Fig 4 is very difficult to understand: what if you would swap Fig 4 and Fig 5? Beginning with the zoom, it would be much easier to understand the heavy full segment 1 overview. Why is the dropsonde at different places? Were there two different dropsondes? Please explain.

We have removed the dropsonde winds in the revised manuscript, and solely focus on the DAWN wind profiles and the APR-2 reflectivity. In answer to your question: The dropsondes were released from the DC-8 at intermittent

times, typically after a DC-8 turn maneuver, and where possible away from glaciated clouds where the dropsonde might have iced-up and returned only a partial profile. Whereas DAWN operates on a constant cycle, rotating its optics in the manner mentioned in Figure 1, staring for a period, moving to the next position, etc. DAWN and dropsonde locations will not necessarily coincide. At some times, more dropsondes were released than at others.

Line 225 and caption of Fig 8: explain why you think the convection is growing.

The features noted in the APR-2 Ka-band reflectivity profile near scan 125 indicate a narrow cell with enhanced mid-level reflectivity (ie, maximum is not concentrated in a radar bright band as would be typical of a more stratiform type rainfall phase), and reflectivity starting to push up at or above the approximate 0-degree C freezing level. We (i.e., APR-2 radar operators during CPEX) often noted this feature from the window of the DC-8, a typical picture is shown in Figure 3. On a side note: Note that in Figure 9 (in the revised manuscript) there are 3-4 small cells. Do these organize themselves and develop further, or does the organization fail to hold and the vertical growth dies out? This was one of the questions posed in the original NASA announcement of opportunity (AO) for the CPEX campaign. The DC-8 was not on-station long enough to track this particular evolution. The bigger scientific question of organization of mesoscale convection is largely still an open question, see for example the invited presentation on this by Dr. Ed Zipser (one of the CPEX PI's) from the Fall American Geophysical Union (AGU-2019), available online:

https://agu.confex.com/agu/fm19/meetingapp.cgi/Paper/491084

https://www.youtube.com/watch?v=gbsWSXVwWJc

Fig 15: Is green still the dropsondes? So there are many more dropsondes on this day? Please explain.

We have removed the dropsonde winds in the revised manuscript, and solely focus on the DAWN wind profiles and the APR-2 reflectivity. In answer to your question: green barbs are always meant to refer to dropsonde profiles and red barbs the DAWN wind profiles. DAWN data processing produced 616 profiles for June 10 and 465 profiles for June 11. 26 dropsondes were provided for June 10, and 28 on June 11. On-station times for both dates were not significantly different.

Technical corrections

Line 45: 2x "associated", and verb is missing. Fixed.

Line 107: remove "highly capable". Removed.

Line 110: " a constant 30° elevation angle", I do not understand, you mean probably an off-nadir angle of 30°.

DAWN can position its beams in both elevation and azimuth angle. For CPEX, the elevation angle was fixed at 30-degrees, and the azimuth angle was varied. What you say is another way of phrasing the same thing, we have made mention of this.

Fig 2: the GOES image in the expanded box is very coarse, it should be available at much higher resolution if this is a visible imagery, and lat/lon indications would make the big image easier to interpret. Also, highlight the 4 segments from sections 3.1 - 3.4.

We have replaced all background imagery on all of the figures in the manuscript with higher-resolution GOES-16 visible imagery, which improves the identification of the cloud features (all flights were during daylight hours). The DC-8 flight track during each of the four segments are provided on Figures 4, 10, 13 and 16, respectively. If we also show these on Figure 2, it unnecessarily clutters up the figure with detail that is presented anyhow later on. We added wording that the individual flight track segments from Figure 2 are shown right before the beginning of Section 3.1.

Lines 160 and 176: the unit dB is probably wrong when characterizing a DAWN SNR level.

A logarithmic scale (dB) is an appropriate scale for characterizing the SNR in the DAWN LOS signal power.

Line 185: “show the LOS projections to msl from the DC-8” MSL= capitalized. Fixed.

Fig 5: in the upper panel there are no winds, and in the lower panel there is no dropsonde, so you may want to adapt both lower left text boxes. As mentioned, dropsonde analysis was removed. Fixed.

Fig 6: I do not see any dropsonde, so you may want to adapt both lower left text boxes. As mentioned, dropsonde analysis was removed. Fixed.

Line 249: “winds (not shown)”, you could refer to Fig 6, showing a region quite close where the winds are shown.

The updated manuscript shows DAWN winds at the 2- and 8-km levels, so this is addressed.

Line 256: “of the DAWN. . .” Fixed.

Figs 9, 11, 13 and 15: the color bar is too large. Fixed.

Line 393: 2x “examine” Fixed.

Joint Analysis of Convective Structure from the APR-2 Precipitation Radar and the DAWN Doppler Wind Lidar During the 2017 Convective Processes Experiment (CPEX)

F. Joseph Turk[1], Svetla Hristova-Veleva[1], Stephen L. Durden[1], Simone Tanelli[1], Ousmane Sy[1], G. David Emmitt[2], Steve Greco[2], Sara Q. Zhang[3]

[1]Jet Propulsion Laboratory, California Institute of Technology, Pasadena CA 91107 USA
[2]Simpson Weather Associates, Charlottesville VA 22902 USA
[2]Global Modeling and Assimilation Office (GMAO), Goddard Space Flight Center, Greenbelt MD 20771 USA

Correspondence to: F. Joseph (Joe) Turk (jturk@jpl.caltech.edu)

Abstract. The mechanisms linking convection and cloud dynamical processes is a major factor in much of the uncertainty in both weather and climate prediction. Further constraining the uncertainty in convective cloud processes linking 3-D air motion and cloud structure through models and observations is vital for improvements in weather forecasting, and understanding limits on atmospheric predictability. To date, there have been relatively few airborne observations specifically targeted for linking the 3-D air motion surrounding developing clouds to the subsequent development (or non-development) of convective precipitation. During the May-June 2017 Convective Processes Experiment (CPEX), NASA DC-8-based airborne observations were collected from the JPL Ku/Ka-band Airborne Precipitation Radar (APR-2) and the 2-um Doppler Aerosol Wind (DAWN) lidar during approximately 100 flight hours. For CPEX, the APR-2 provided vertical air motion and structure of the cloud systems in nearby precipitating regions where DAWN is unable to sense. Conversely, DAWN sampled vertical wind profiles in aerosol-rich regions surrounding the convection, but is unable to sense the wind field structure within most clouds. In this manuscript, the complementary nature of these data are presented from the June 10-11 flight dates, including the APR-2 precipitation structure and Doppler wind fields, and adjacent wind profiles from the DAWN data.

Deleted: e

Deleted: sampling

Deleted: convective cloud processes linking

Deleted: and transport of water vapor near

Deleted: , and the

Deleted: . Frequent dropsonde data accompanied the DAWN observations for validation purposes, and to provide complement wind profiles in and near convection.

Deleted:

Deleted: and dropsonde

1 Introduction.

The mechanisms linking convection and cloud dynamical processes is a major factor in much of the uncertainty in both weather and climate prediction. The associated mesoscale convective systems (MCS) produce much of the Earth's rainfall and are responsible for the bulk of the heat and moisture transport from the Earth's surface into the upper troposphere. The cold pool dynamics are thought to be an important mechanism to facilitate the development of MCSs in the tropical atmosphere (*Chen et. al*., 2015; *Zuidema et. al*., 2017), as well as interactions between individual isolated convective storms (*Raymond et. al.,* 2015). These atmospheric boundaries can have significant impact on deep convection, affecting its

initiation, updraft strength and longevity. The intensity and size of the cold pools is strongly dependent upon the vertical distribution of the temperature and humidity and the vertical shear of the horizontal wind. While the overall processes responsible for these interactions have been identified for some time, their precise nature and interactions remains under-constrained by observations, due to the difficulty in obtaining accurate, vertically resolved pressure, temperature, wind and water vapor in the proximity of developing convective clouds. Moreover, increasing evidence points to control of convection by the relatively smaller and more variable amount of moisture above the boundary layer, in the free troposphere (*Schiro and Neelin*, 2019). Further constraining the uncertainty in convective cloud processes *linking 3-D air motion and cloud structure* through models and observations is vital for improvements in weather forecasting and understanding limits on atmospheric predictability.

The resolution of the precipitation radar onboard the Tropical Rainfall Measuring Mission (TRMM; 1997-2014) and the subsequent Global Precipitation Measurement (GPM; 2014-current) missions (4-km horizontal resolution; 250-m vertical) have enabled numerous observational-based studies of MCS convective structure and features (*Jiang et. al*., 2011). However, the dynamical (air motion) wind field associated with MCS features at this scale not well-represented by current space-based wind profile observing capabilities. The majority of available atmospheric wind observations are primarily water vapor and cloud-tracked atmospheric motion wind vectors (AMV) derived from operational geostationary satellites (*Velden et. al*, 2005), which can be refreshed as quickly as 15-minutes, but are mainly indicative of large-scale mid-to-upper level air motion patterns. Observations of wind vectors in the periphery of smaller-scale cloud systems, especially in the 2-km nearest the Earth (the approximate delineation of the boundary layer) are much less abundant. Outside of ground-based profiling networks, very few over-ocean wind profile observations at a similar GPM-like horizontal resolution are available.

A space-based Doppler wind lidar (DWL) capability has been envisioned as one means to overcome this observational shortcoming (*Baker et. al*., 2014). Over the past decade, airborne DWL field campaigns have been conducted (*Lux et. al*., 2018), recently in preparation for the deployment (August 2018) of the first-ever spaceborne DWL, the Atmospheric Dynamics Mission (ADM-Aeolus) of the European Space Agency (ESA) (*Stoffelen et. al*., 2005). Aeolus provides vertical profiles of the horizontal line-of-sight (LOS) winds at an ≈100-km horizontal resolution and 200-km separation between profiles, with a main application to numerical weather prediction data assimilation (*Horányi et. al.*, 2015). Observations from campaigns with a DWL such as the THORPEX Pacific Asian Regional Campaign (TPARC) were largely focused towards improvement of tropical cyclone forecasts (*Pu et. al*., 2010). These airborne campaigns have validated the capabilities of a DWL to provide wind profiles in the boundary layer (*Bucci et. al*., 2018; *Zhang et. al*., 2018). There has been relatively less focus in collection and analysis of airborne DWL observations in relation to the convective processes linking air motion and transport of water vapor near clouds, and the subsequent development (or non-development) of convection. One main reason is that previous campaigns often lacked nadir scanning Doppler precipitation radar capabilities on the same aircraft to enable matched radar-DWL observations. A scanning precipitation radar provides the

Deleted: associated

Deleted: at

Deleted: TRMM/GPM-like

Deleted:

Deleted: approximate

actual 3-D representation of the condensed water mass field, and the vertical Doppler winds and associated microphysical vertical structure (*Rowe and Houze*, 2014; *Rowe et. al*., 2012). These data provide one means to validate the forecasted model precipitation structure (e.g., presence/absence of convection, timing, location), that results when the DWL wind vectors are assimilated into cloud resolving models.

In this manuscript, airborne DWL and Doppler precipitation radar observations are presented from the NASA-sponsored Convective Processes Experiment (CPEX), which took place between 25 May and 24 June 2017, based out of Fort Lauderdale, FL. The goals of CPEX were to improve the understanding of convective processes during initiation, growth, and dissipation, using a combination of observations and cloud-resolving models. In particular, to measure what combinations of environmental structure and observed convective properties such as vertical velocity and reflectivity profiles, result in rapid upscale growth of a convective system into a large organized mesoscale convective system (MCS), or alternatively, result in failure to grow or rapid decay. This manuscript will describe and present only the airborne precipitation radar and DAWN observations; a separate manuscript will present the associated mesoscale model simulations and DAWN data assimilation experiment results (*Zhang et. al.*, 2019).

Deleted: DWL

Deleted: DWL

2 CPEX Overview.

During CPEX, sixteen NASA DC-8 airborne missions were flown into the Gulf of Mexico, Caribbean Sea and the Atlantic Ocean. Each date is summarized in Table 1. During each flight, joint observations were collected from the JPL Ku/Ka-band Airborne Precipitation Radar (APR-2)[1] and the 2-um Doppler Aerosol Wind (DAWN) lidar, covering a variety of isolated, scattered, and organized deep convection, totalling approximately 100 flight hours. Intermittent dropsonde data accompanied the DAWN observations for validation purposes, and to provide complementary wind profiles near convection. The dropsondes system used during CPEX was the High Definition Sounding System (HDSS) dropsonde delivery system developed by Yankee Environmental Services (*Black et. al*., 2017). The dropsonde data are not presented in this manuscript.

Deleted: DWL

Deleted: Frequent

Deleted: While t

Deleted: are shown on several of the following figures, they

Deleted: discussed

Flight	Date	Observations
1	27 May 2017	First local science flight; box pattern in central Gulf; clear air only.
2	29 May 2017	Sampling of scattered convection in NW Caribbean; cells at 1813, 1942-2000.
3	31 May 2017	Multiple boxes over Atlantic, near Bahamas and north of Hispaniola; mostly clear but cells at 1936, 2120.
4	1 June 2017	Convective system over eastern Gulf; multiple passes over convection. 25-min data loss at Ka-band due to TWT amplifier breaker trip.

[1] In 2015, APR-2 was augmented with an additional W-band (94 GHz) Doppler radar for an expanded APR-3 capability. Owing to logistical details, the W-band radar was unavailable for CPEX in 2017, hence the use of the APR-2 system.

5	2 June 2017	Extended E-W box over western and central Gulf; clear areas and some convective cells, for example at 1750, 1928; decaying convection between 1830-1900, 2100-2110.
6	6 June 2017	Convection over eastern Gulf, especially near 1858, 1955-2115, 2105, 2140.
7	10 June 2017	Boxes east of the Bahamas; stratiform with some convection on ascent between 1840-1850, small cells in box 1925, 2004, 2035-2045, 2118, 2140, 2210-2216.
8	11 June 2017	E-W legs over convective system in central Gulf; isolated cells at 1801, 1830, 1850; extensive precipitation on lines starting at 1900, 1920, and N-S line starting 2005.
9	15 June 2017	Caribbean, east of Yucatan; convection near 1920, 1940, 1953, 2010.
10	16 June 2017	Caribbean, boxes east of Yucatan; convection near 1830-1940, 2050-2140.
11	17 June 2017	Caribbean, boxes east of Yucatan; convective cells at 1745, 1800-1815, 2044-2054, 2223; sampled convective system with box pattern between 1900 and 2030.
12	19 June 2017	E-W legs over north-central and northeast Gulf of Mexico, Tropical Storm Cindy; extensive precipitation between 1700-1820, 1840-2005; numerous isolated cells to 2130, then more extensive areas to 2224.
13	20 June 2017	Bow-tie pattern in central Gulf of Mexico; convective system between 1742-1754, cells 1815-1820, very shallow convection 1923, extensive precipitation between 2110-2150.
14	21 June 2017	E-W flight across Gulf of Mexico; isolated cells at 1842, 1942, 2028, 2107, 2124, 2158, 2240; stratiform/transitional between 1925-1937.
15	23 June 2017	Box pattern to east of Bahamas; crossed isolated cells at 1832, 1859, 1910, 1917; multiple lines over area with isolated cells between 1912-1939.
16	24 June 2017	Over and around Cuba; convection at 1744, box pattern cells near 1829, isolated cells 1843-1944; mature cell near 2106, more cells 2112-2143.

Table 1. Summary of CPEX flight dates.

APR-2 is a 2-frequency Doppler radar, originally developed as an airborne prototype for the second-generation GPM/DPR precipitation radar (*Sadowy et al*., 2003). The APR-2 has flown in numerous airborne field campaigns outside of CPEX, most recently the ORACLES (2016-2018) and CAMP2Ex (2019) campaigns. APR-2 acquires simultaneous measurements of multiple parameters at both Ku- and Ka-band (14 and 35 GHz, respectively), including co- and cross-polarized radar backscatter, and LOS Doppler velocities of hydrometeors, with a maximum unambiguous velocity of ±27.5 (Ku-band) and ±10.4 (Ka-band) m s^{-1}. From a nominal 10-km flight altitude, the horizontal resolution at the surface is ~800-m, with a vertical range resolution and sampling of 50- and 30-m (slightly oversampled). Based upon analysis of radar surface backscatter measurements from CPEX, the reflectivity calibration is accurate to within 1-2 dB. From these basic measurements, APR-2 can depict the cloud macroscopic structure (extent, vertical air motion) and estimate the microphysical structure (water content, precipitation intensity, hydrometeor size distribution) of the associated precipitation (*Durden et. al.*, 2012). These resolutions are adequate to capture cloud features down to the resolution typical of high-resolution cloud models, and appropriate for comparison with DAWN wind profiles in the vicinity near isolated, scattered, and organized deep convection.

DAWN is NASA's airborne DWL with a 2-micron laser that pulses at 10 Hz (*Kavaya et. al*., 2014). It has previously participated in the NASA Genesis and Rapid Intensification Processes (GRIP) (2010) and Polar Winds (2014-15) airborne campaigns. DAWN can provide high resolution (4-12 km in the horizontal and 35-150 m in the vertical) wind measurements in clear as well as partly cloudy conditions. The lidar samples the scene in a conical pattern at a constant 30º elevation angle (i.e., 30-degrees off of nadir), and collects LOS wind profiles at up to five azimuth angles located at -45º, -22.5º, 0º, 22.5º and 45º relative to the aircraft flight direction (Figure 1). During CPEX, DAWN also collected LOS data at only two azimuth angles, -45º and 45º. Since these LOS wind profiles view the local wind field from multiple azimuth angles, multiple LOS profiles are analyzed to estimate the vertical profile of the horizontal wind components (*u, v*) at different pressure levels using the Adaptive Signal Integration Algorithm (ASIA) processing (*Kavaya et. al.,* 2014). DAWN data are available in both the native LOS format, and processed wind vector (*u, v*) profile format. In this manuscript, the wind vector data are used to evaluate the wind field near clouds captured by the APR-2. The individual LOS data are projected (along the viewing direction) through the APR-2 radar scan to illustrate the ability of DAWN to sense in and near cloud structures.

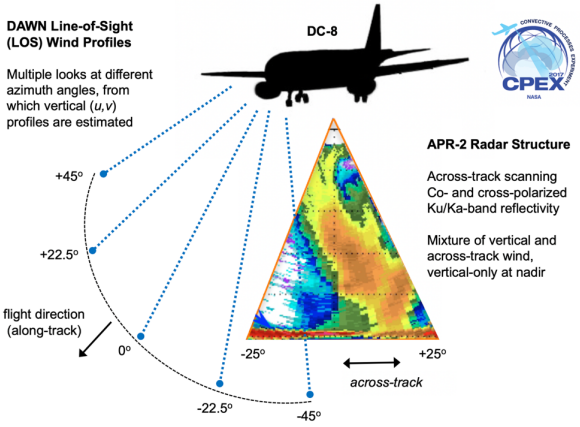

Figure 1: Depiction of DAWN and APR-2 scanning operations from the DC-8 during CPEX. From a 10-km flight altitude, the APR-2 across track swath width is 8-km, which is approximately the same distance as the separation between the DAWN ground locations of the -45- and +45-degree LOS profile beams.

Deleted: highly capable

Deleted: gathers

Deleted: data

Deleted: these

Deleted: analyzed

Deleted: profile

Deleted: , and the

Deleted: were

Deleted: evaluate

Deleted:

Deleted: along the LOS profile

3 DC-8 Flight Segments on 10 June 2017.

The intent of this section is to assess the DAWN sampling density near the cloud systems captured by the APR-2, relative to the cloud evolution. The 10 June 2017 case is highlighted in this section. This case is used since it is a fairly isolated cloud growth case, not greatly affected by large-scale forcing at early stages, and was covered by several repeat DC-8 passes from various directions. On 10 June 2017, the DC-8 took off from Fort Lauderdale near 1800 UTC and headed east towards the area of interest (AOI) with building clouds, located in the box bounded between 24.2N-26.2N latitude and 74W-72W longitude. Figure 2 shows the DC-8 flight tracks on this date, taken from the JPL CPEX Data Portal (**http://cpex.jpl.nasa.gov**) (*Hristova-Veleva et. al*., 2019), superimposed upon GOES-16 geostationary visible channel imagery from 1902 UTC.

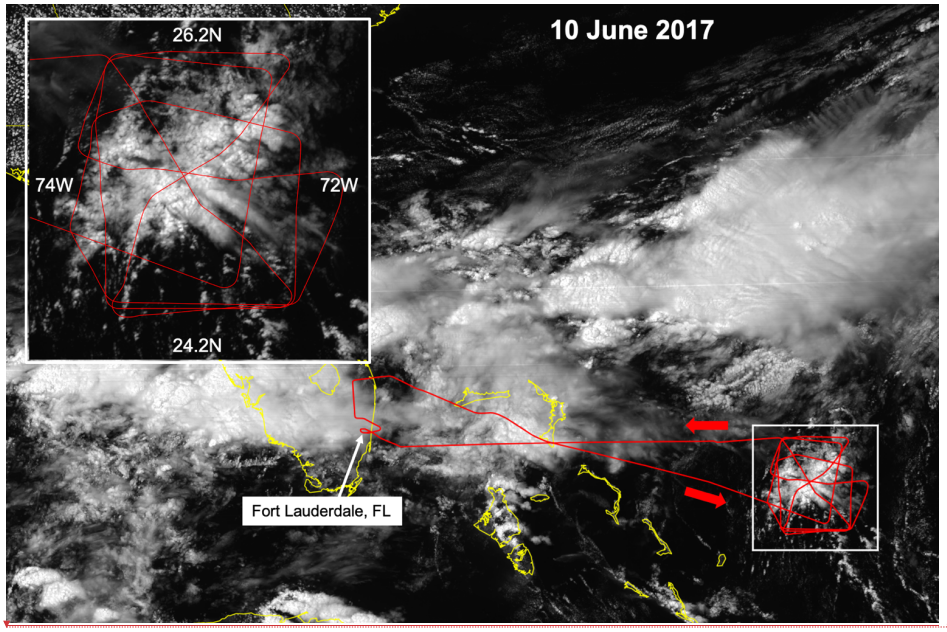

Figure 2: 10 June 2017 flight track (red lines), shown on the JPL CPEX data portal. The DC-8 home base at Fort Lauderdale, FL is indicated. The main area-of-interest is shown in the expanded box, covered by the DC-8 during the 1830-2230 UTC time period. The grayscale background depicts the GOES-16 visible imagery at 1902 UTC.

Deleted: superimposed upon GOES-East geostationary visible channel imagery from 2000 UTC …

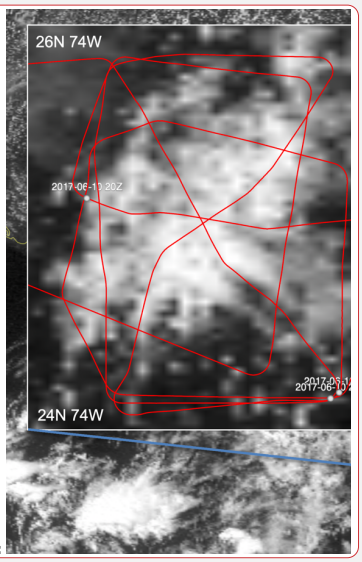

Deleted:

Deleted: East

Deleted: near

Deleted: 2000

A series of convective box patterns were executed, to sample the evolution of the air movement surrounding the convection from multiple flight bearings. The intent was to be on-station in order to capture developing cumulus clouds before they had developed any significant glaciation, before they reached a stage of vertical development where the DC-8 was unable to overfly from its nominal 10-km flight altitude. A photograph taken from the DC-8 near 2200 UTC (Figure 3) on this date illustrates an example of a cloud at a desired stage of evolution, where the clouds are captured at an early enough stage such that the DC-8 can safely overfly multiple times during subsequent evolution.

Figure 3: View of developing cumulus from the DC-8 window, near 2200 UTC on 10 June 2017, from a 10-km flight altitude.

APR-2 data was collected in tandem with DAWN between 1835-2230 UTC. To explain the DAWN observations relative to the development of the precipitation, the analysis is broken into four one-hour segments, separated by the DC-8 flight track segments during each hour. The APR-2 data will be shown in context to give a sense of when and where (proximity and cloud penetration depth) DAWN can provide valid wind data. Furthermore, the analysis will focus on the wind shear within

Deleted: any

Deleted: in each of the sub-sections below

each quadrant (NE=northeast, SE=southeast, SW=southwest, NW=northwest), relative to the approximate center (25.2N 73W) of the AOI flight box in Figure 2. These segments also correspond to the data assimilation interval used in the investigation of these data by *Zhang et. al*. (2019).

3.1 Flight Segment 1 (1830-1930 UTC).

This first DC-8 flight segment flew along a 120-degree bearing approaching the NW and SW quadrants of the AOI, whereas the next three flight segments discussed below take place inside of the main AOI. Figure 4 shows the plan view at 2-km (top) and 8-km (bottom) constant elevation levels. The locations of DAWN wind vectors are shown by the red barbs. The densest DAWN sampling occurs between 1900-1930 in the mostly cloud-free area, shown in the lower right of Figure 4, with 5-10 m s^{-1} winds at both levels.

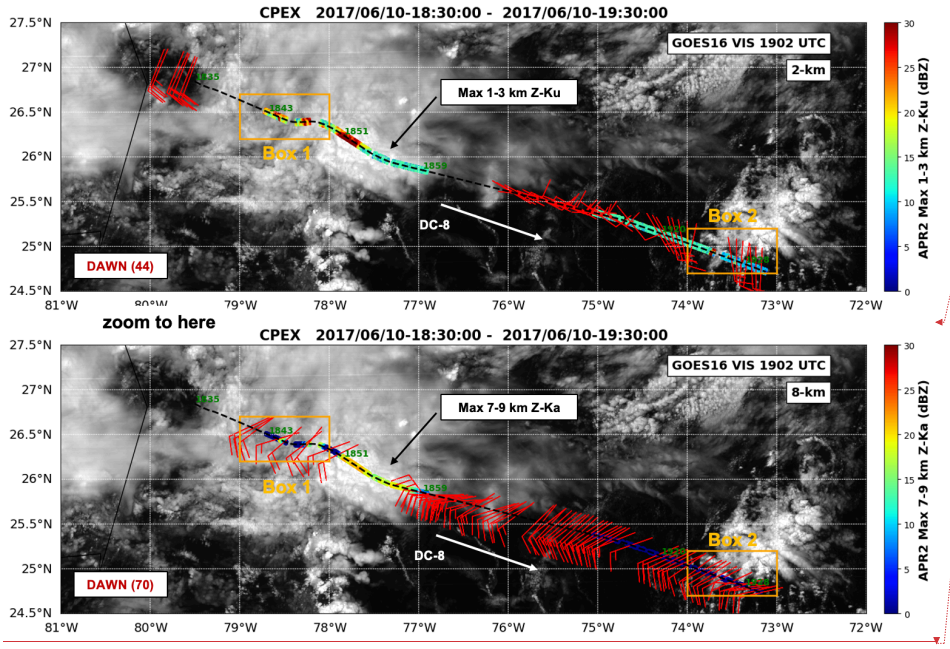

Figure 4. DC-8 flight line during segment 1 (1830-1930 UTC) on 10 June 2017. The GOES-16 visible imagery at 1900 UTC is shown in the background grayscale (scaled from 0-100% albedo, not shown). (Top panel): The red barbs show the locations of the wind vectors (44 total) estimated by DAWN at 2-km height. The background color represents the average APR-2 Ku-band

Deleted: collected data approaching the outside …W and SW... [1]

Moved down [4]: The locations of the DAWN LOS profiles are indicated with colored markers, which owing to the conical scan pattern of the five looks shown in Figure 1, appear as a zig-zag

Moved down [2]: The grayscale background indicates the GOES-13 geostationary 11 μm infrared (IR) temperature

Moved down [3]: The densest sampling occurs between 1900-1930 in the mostly cloud-free area, shown in the lower right of Figure 4 with 5 m s^{-1} winds at both levels. The grayscale

Deleted: The grayscale background indicates the GOES-13 geostationary 11 μm infrared (IR) temperature (white=cold ... [3]

Moved (insertion) [3]

Deleted: During this time the cloud and aerosol conditions were such that the processing of the DAWN LOS data produced a total of ... [2]

Deleted: The locations of these vectors are shown by the red wind barbs. …

Moved (insertion) [2]

Deleted:

Moved down [1]: There is a tendency for increased directional shear between these levels as the DC-8 approaches the AOI.¶

Deleted: ¶

Formatted: Caption

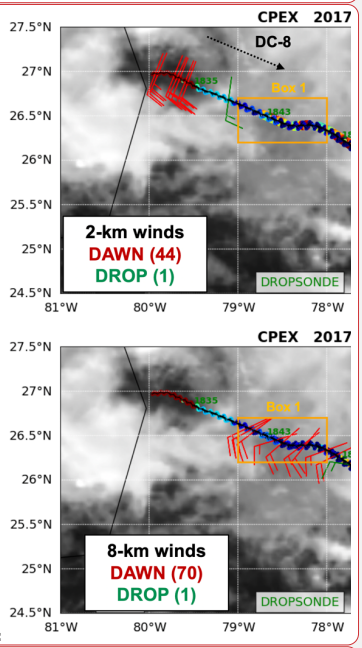

Deleted:

Deleted: Segment 1 (1830-1930 UTC) on 10 June 2017. The ... [4]

reflectivity between 1-3 km height (top color scale). (Bottom panel): Same as top panel, but for an 8-km height. The background color represents the APR-2 average Ka-band reflectivity between 7-9 km (bottom color scale).

For the 2-km level, the maximum APR-2 Ku-band reflectivity between 1-3 km is plotted underneath the DAWN winds; for the 8-km level the maximum Ka-band reflectivity between 7-9 km is shown instead (the rationale being that since there is less path attenuation through rain at Ku-band than at Ka-band, the Ku-band data provide a better depiction of the cloud structure for the deeper 2-km level; the APR-2 is more sensitive to clouds at Ka-band than at Ku-band, so the Ka-band reflectivity was used for the higher 8-km level cloud structure). Peak APR-2 Ku-band reflectivity at 2-km exceeded 30 dBZ.

In Figure 4, the associated cloud and aerosol conditions were such that the processing of these DAWN LOS data produced a total of 44 vectors at 2-km height (top), and 70 vectors at 8-km height (bottom). To look in more detail to the DAWN sampling proximity relative to the locations of individual cloud structures sampled by the APR-2, Figure 5 and Figure 6 show zoom-in depictions covering the two boxes indicated with the orange rectangles in Figure 4, which cover a mostly cloudy area (Box 1 from 1835-1855 UTC, Figure 5) and mostly clear area (Box 2 from 1924-1930 UTC, Figure 6), respectively. The mean sea level (MSL) locations of the DAWN LOS profiles are indicated with colored markers. Owing to the conical scan pattern of the five looks shown in Figure 1, the locations appear as a zig-zag pattern as the DC-8 moves forward. Each DAWN LOS beam is colored by the lowest altitude where the SNR > 5 (the 5-dB value is used as a reference level, not as an absolute minimum threshold, as DAWN often provides valid data at lower SNR levels). The ground locations of the DAWN LOS profiles are indicated with colored markers, and a thin line connected to each marker shows the LOS projection extending from the DC-8 to MSL.

Deleted: 2-4

Deleted: all DAWN and dropsonde data are

Deleted: The

Deleted: m is shown under each DAWN LOS location

Deleted: Note the increased sampling density between 1900-1930 UTC.¶

Moved (insertion) [1]

Deleted: There is a tendency for increased directional shear between these levels as the DC-8 approaches the AOI.¶

Deleted: precipitation

Deleted: 5

Deleted: 6

Moved (insertion) [4]

Deleted: , which

Deleted: o

Deleted: (this pattern will be more obvious in Figures 5 and 6)

Deleted: In both Figures 5 and 6, the top panel (2-km level) shows the maximum APR-2 Ku-band reflectivity between 1-3 km plotted underneath the DAWN LOS locations; in the bottom panel (8-km level) the maximum Ka-band reflectivity between 7-9 km is shown instead (the rationale being that since there is less path attenuation through rain at Ku-band than at Ka-band, the Ku-band data provide a better depiction of the cloud structure for the deeper 2-km level; the APR-2 is more sensitive to clouds at Ka-band than at Ku-band, so the Ka-band reflectivity was used for the higher 8-km level cloud structure). Peak APR-2 Ku-band reflectivities at 2-km exceeded 30 dBZ.

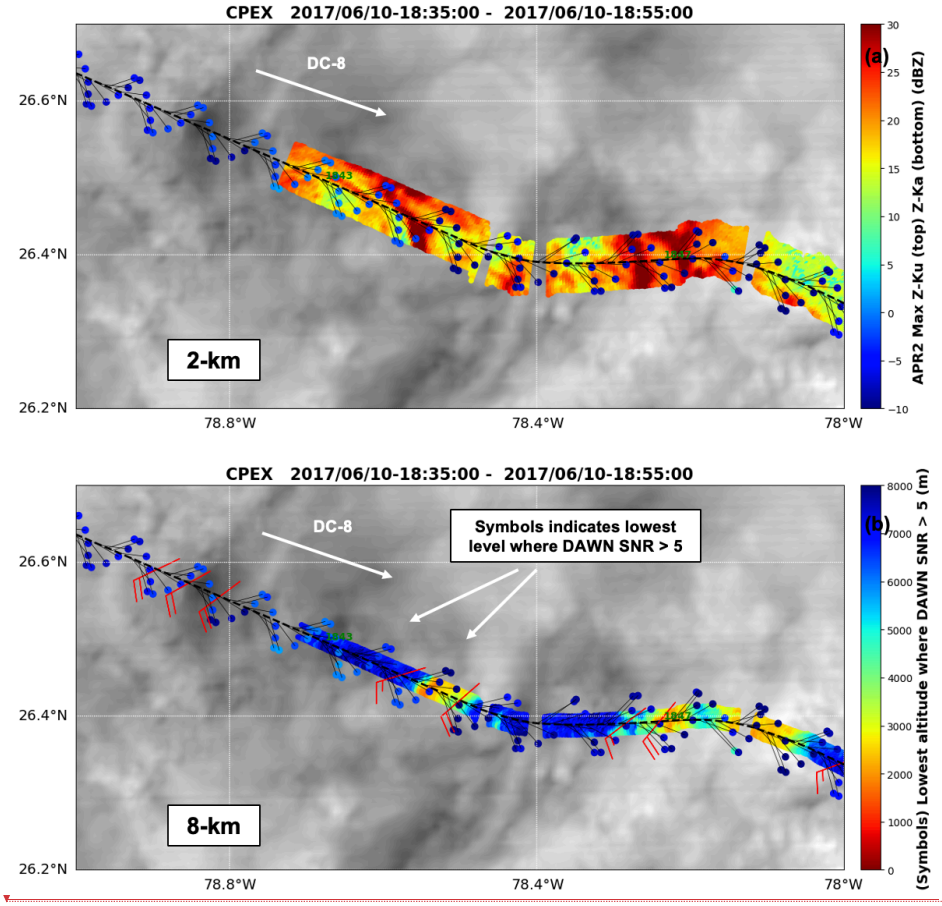

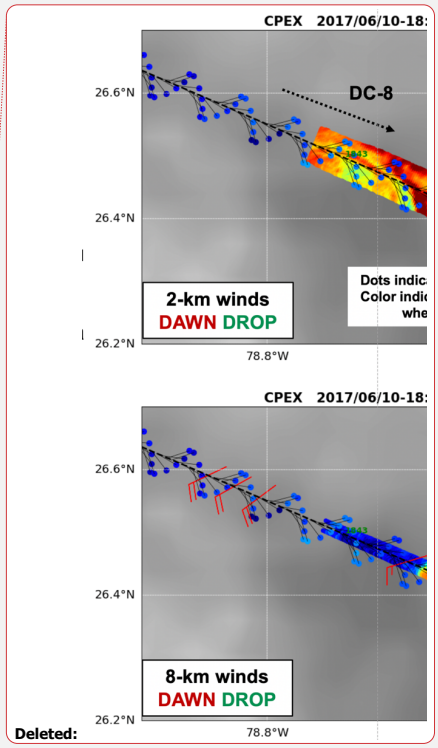

Figure 5. Same as Figure 4, but zoomed in to the flight segment between 1835-1855 UTC (Box 1 in Figure 4). The symbol (dot) colors indicate the lowest level where DAWN SNR > 5 dB (lower panel color scale). Periods of missing APR-2 data indicate no data. (a) 2-km level, (b) 8-km level. DAWN winds at each level are indicated with the red barb symbols.

Note that in the mostly-cloudy Box 1 area (Figure 5), the DAWN sampling pattern is evident, covering about an 8-km swath as the lidar collects samples at each of the five azimuth locations in its conical scan. For these cloud cover conditions, no

DAWN wind vectors were estimated at the 2-km height. However, at 8-km height, DAWN processing retrieved wind vectors even where the Ka-band reflectivity in the vicinity was as high as about 15 dBZ, showing about 10 m s^{-1} south-easterly winds. The mostly-clear Box 2 region shown in Figure 6 (1924-1930 UTC) is presented in an identical layout as Figure 5. At this time, DAWN was configured in the 2 looks per scan (-45° and 45° azimuth). In this region, DAWN was able to sense well below 2-km even in the vicinity of clouds at the 10-15 dBZ Ku-band reflectivity level from APR-2, showing 5 m s^{-1} southerly winds at 2-km, becoming more westerly at 8-km height.

Deleted: However

Deleted: southeasterly

Deleted: ¶
¶

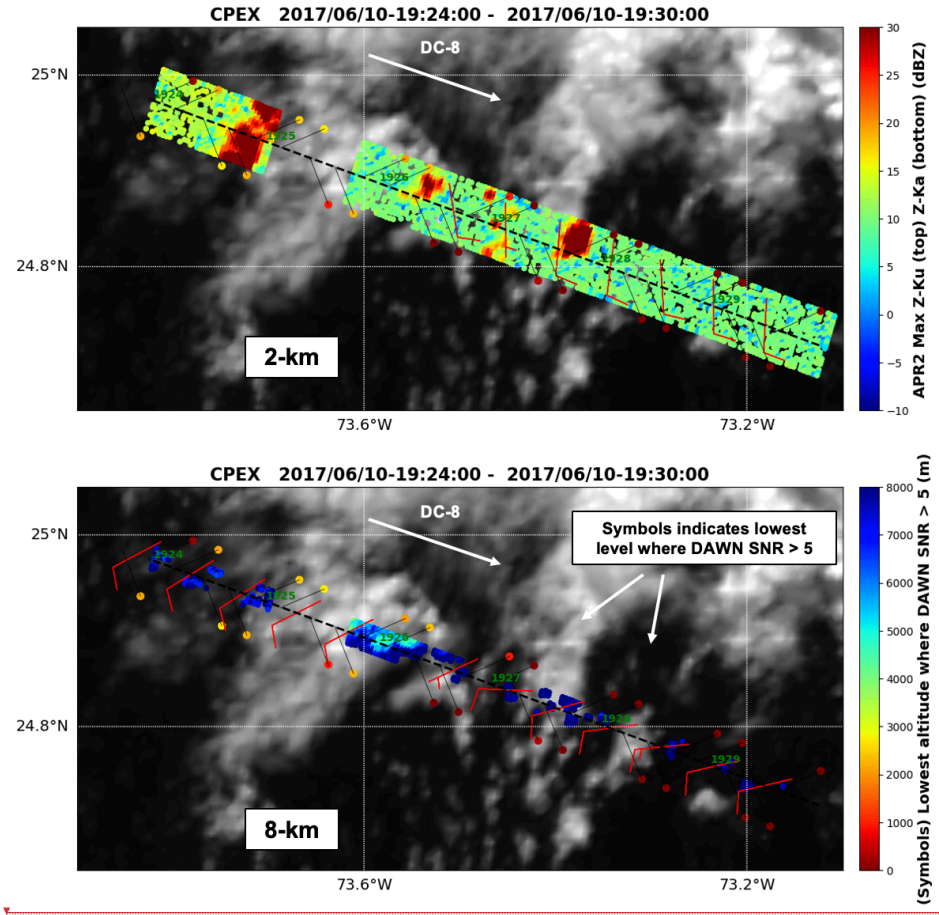

Figure 6. Same as Figure 5, but zoomed in to the flight segment between 1924-1930 UTC (Box 2 in Figure 4).

In these DAWN data, there is a tendency for increased directional shear between these two vertical levels as the DC-8 approaches the AOI. To enhance this feature, the left panel of Figure 7 displays each DAWN profile in Figure 4 in a two-level hodograph form, where each vector points from the DAWN (u,v) wind at 2-km to the (u,v) at 8-km, thereby

Deleted:

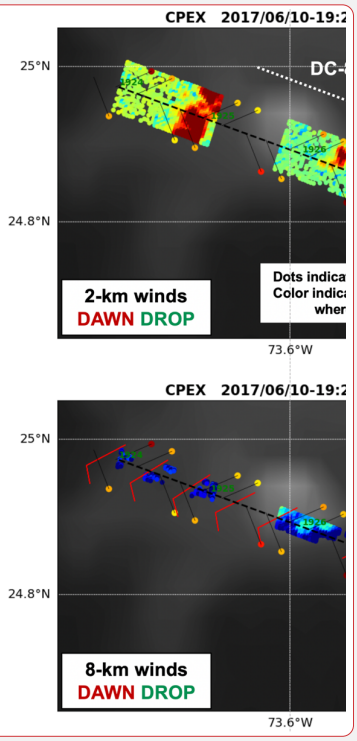

Deleted: 6

Deleted: 4

Deleted: ¶

representing the shear between these two levels. When the vector is aligned along a radial direction, that indicates no directional shear, only speed shear. When the vector is aligned away from the radial direction, that indicates directional shear and possible speed shear. The shear vectors are colored according to which quadrant (NE, SE, SW, NW) they are located in, relative to the approximate center (25.2N 73W) of the AOI flight box in Figure 2. During this time there is sustained directional wind shear in the SW and NW quadrants, oriented from west to east. A similar analysis for the shear between 2-km and 6-km (right panel of Figure 7) shows the shear oriented more south to north.

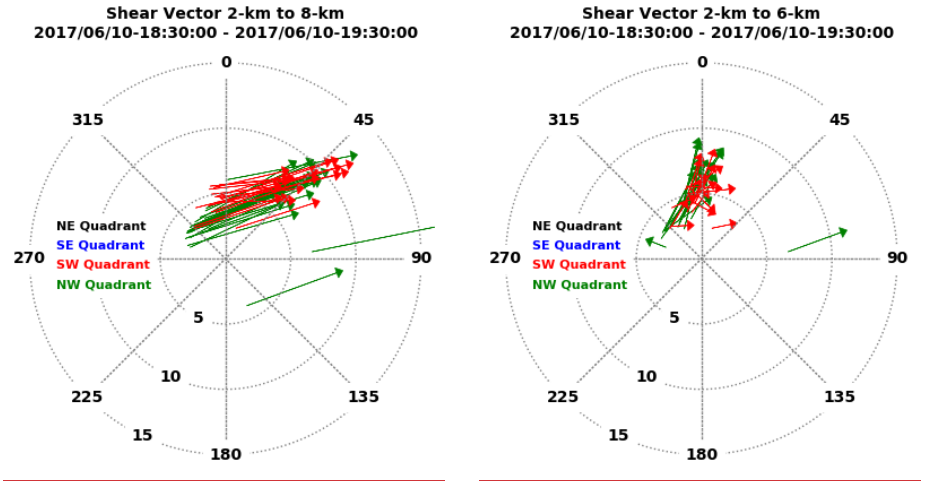

Figure 7. Two-level hodograph derived from the DAWN wind profiles during 1830-1930 UTC in a polar coordinate form. Rings are spaced at 5 m s^{-1} intervals. Each vector represents shear derived from each wind profile. (Left) Shear vector pointing from (*u*,*v*) at 2-km towards (*u*,*v*) at 8-km. (Right) Shear vector pointing from (*u*,*v*) at 2-km towards (*u*,*v*) at 6-km. The shear vectors are colored according to which quadrant (NE=northwest, SE=southeast, SW=southwest, NW=northwest) they are located in, relative to the approximate center (25.2N 73W) of the AOI flight box in Figure 2. During this time, the DC-8 sampled only the SW and NW quadrants.

To provide a depiction of the DAWN vertical sampling capability, a cross-section of the DAWN vertical profile sampling locations superimposed upon the APR-2 nadir reflectivity is shown in Figure 8. The black points represent locations of valid DAWN (*u, v*) wind vectors during this time. Several notable features are evident. Depending upon the APR-2 transmit pulse length, there is a blind zone (~ 1.8 km) below the aircraft where the radar processor does not receive any returned signals. This is noted in a short period where the cloud tops were within the APR-2 blind zone (near scan 750), but the

Formatted: Font: 10 pt, Not Bold
Formatted: Font: 10 pt, Not Bold
Formatted: Font: 10 pt, Not Bold
Formatted: Font: 10 pt, Not Bold
Deleted: 7
Deleted: from all DAWN wind profiles
Deleted: DAWN does not have this limitation and provided LOS returns in this missing area. In fact, there…
Deleted: is

cloud top was identifiable in the DAWN profiles (labeled the "upper cloud area" in green shading in Figure 8). Similarly, near the surface where the APR-2 backscatter is affected by ground clutter in the lowest 500-m, DAWN was able to provide wind observations to the surface. In general, DAWN winds are abundant above 6-km (where the SNR is highest), and below 3-km (where the aerosol content is higher), with considerable upper level sampling right up to the edges of the tall developed clouds (near scan 1000). There are several DAWN profiles that bump up close to the small convective cell near scan 1800 (denoted with a red ellipse in Figure 8), which are associated with the clouds shown in Figure 6 (Box 2) top panel, where the Ku-band reflectivity exceed 30 dB. To show this area in more detail, Figure 9 zooms in to the Box 2 area (1924-1930 UTC), where three small growing clouds are shown in the middle of this figure. DAWN wind profiles are produced to the surface next to growing convection near scans 100 and 120, but not for the cell near scan 75. This highlights that convective clouds are not continuous "impenetrable" cloud structures, but in nature have gaps or "holes" in them where the DAWN LOS view can penetrate through to lower levels.

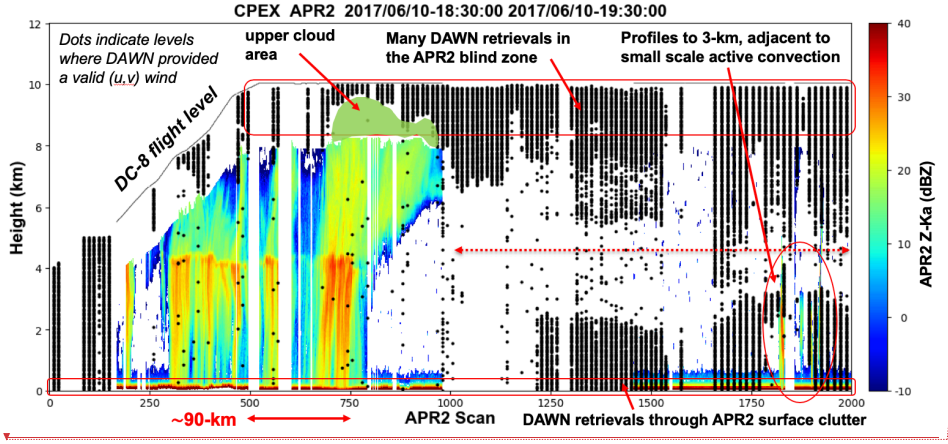

Figure 8. Cross-section of the APR-2 Ka-band reflectivity (color scale in dBZ) during segment 1 (1830-1930 UTC). The x-axis represents the APR-2 scan number (2000 scans representing 720-km ground distance), and y-axis the MSL height (km). The DC-8 reached its nominal 10-km flight altitude near 1840 UTC. The black points represent vertical locations of valid DAWN (*u, v*) wind vectors produced from the DAWN processing of the LOS data. The green shaded "upper cloud" area shows an area where there are clouds in the 1.8-km blind zone (where APR-2 does not process data), but whose cloud top is noted in the DAWN profiles above this shaded area.

Deleted: by the lowest-most level
Deleted: labeled
Deleted: gray
Deleted: 7
Deleted: sense
Deleted: , providing wind observations within the boundary layer
Deleted: 7
Deleted: reflectivities
Deleted: 8

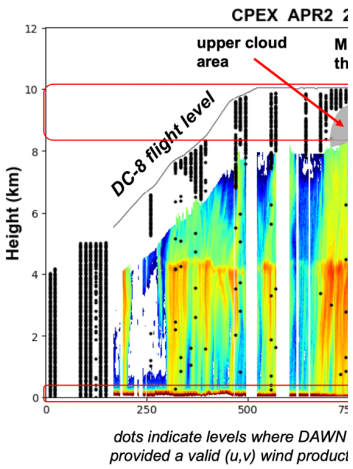

Deleted:
Deleted: 7
Deleted: to right
Deleted: S
Deleted: above the ocean surface
Deleted: wind profiles obtained during
Deleted:
Deleted: gray
Deleted: "
Deleted: "
Deleted: s not receive any
Deleted: by the lowest-most level

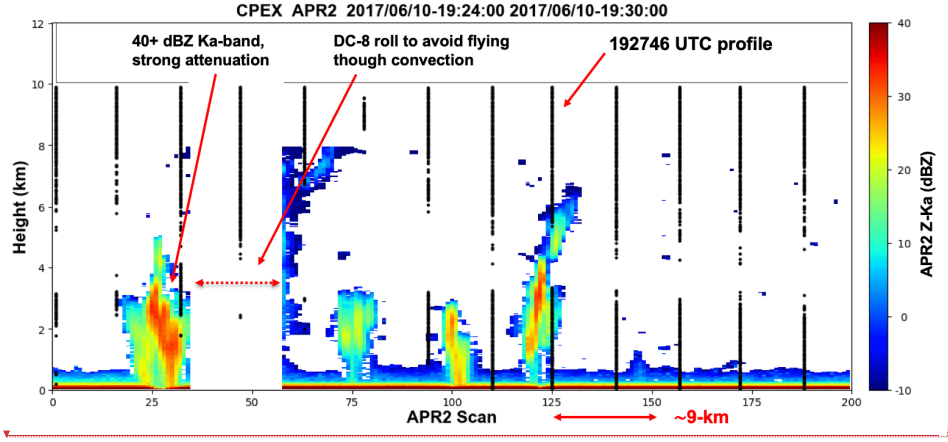

Figure 9. Same format as Figure 8, but covering only the Box 2 area (1924-1930 UTC) shown in Figure 4. DAWN wind profiles are obtained to the surface very close to the growing convection near 192746 UTC (near scan 120).

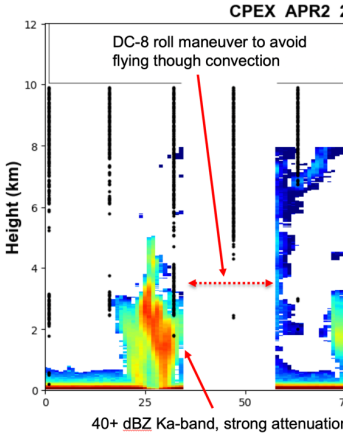

Deleted:

Deleted: 8

Deleted: 7

Deleted: 6

3.2 Flight Segment 2 (1930-2030 UTC).

From 1930-2030 UTC, the DC-8 conducted a series of flight legs in a counter-clockwise pattern within the AOI with densest sampling in the NW and SE quadrants, before departing along a 270-degree bearing. Figure 10 illustrates the APR-2 and DAWN data in the same format as used in Figures 5 and 6. Maximum Ka-band reflectivity in the 7-9 km level are near 20-25 dB in the middle of the segment. On the north side of the AOI, the winds were mainly southwesterly near 10 m s^{-1}, with 2-km level winds more southerly with weaker 5 m s^{-1} speeds.

Deleted: started off along a 120-degree bearing near 25N, then

Deleted: surrounding clouds at 25N 73W

Deleted: before leaving to the south and departing along a 270-degree bearing…

Deleted: .

Deleted: 9

Deleted: DC-8 flight tracks

Deleted: 4, only the 8-km wind level is shown for brevity.

Deleted: reflectivities

Deleted: A total of 38 and 39 DAWN wind vectors were collected at the 2- and 8-km level, respectively, during this time. …

Deleted: (not shown)

Deleted: On the south side of the AOI, there was more directional shear, with 8-km westerly winds and 2-km southerly winds (not shown).

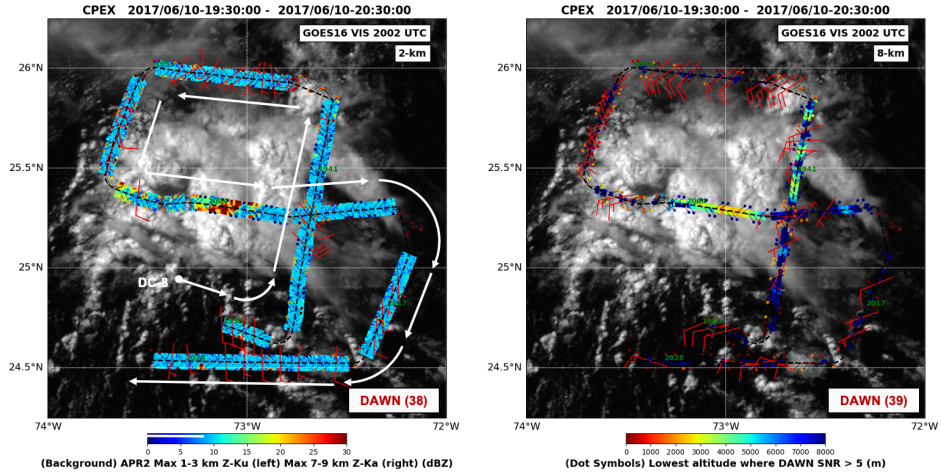

Figure 10. DC-8 flight line during segment 2 (1930-2030 UTC) on 10 June 2017. The GOES-16 visible imagery at 2000 UTC is shown in the background grayscale. DAWN winds at each level are indicated with the red barb symbols. (Left) 2-km level. The background color represents the average APR-2 Ku-band reflectivity between 1-3 km height. (Right): Same as left panel, but for an 8-km height. The background color represents the APR-2 average Ka-band reflectivity between 7-9 km. In both panels, the symbol (dot) colors indicate the lowest level where DAWN SNR > 5 dB (lower panel color scale), according to the color scale on the right panel. Periods of missing APR-2 data indicate no data.

In the NW quadrant of the AOI, there is a large shear magnitude between the 2- and 8-km levels (Figure 11), but it is less directional (vectors more aligned in the radial) compared to Figure 7. In Figure 11, the shear between 2- and 6-km in the NW quadrant (green arrows) is similar to Figure 7, but the shear between 2- and 8-km is pointing more towards the east. The shear between 2- and 8-km in the SW and SE quadrants (red and blue arrows, respectively) points mostly towards the east-southeast directions, but this same signature is not well noted between the 2- and 6-km levels, owing to the reduced DAWN sampling at the 6-km level.

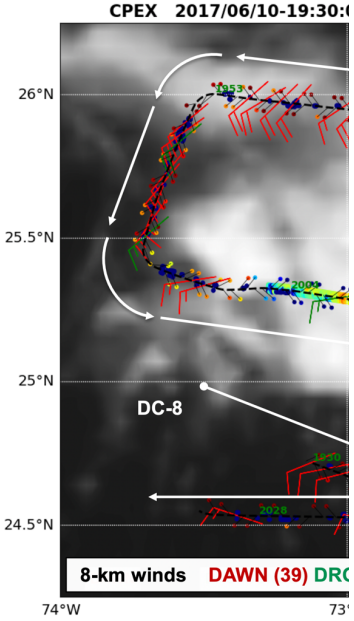

Deleted:

Deleted: 9

Deleted: S

Deleted: East

Deleted: IR

Deleted: (white=cold; black=warm)

Deleted:

Deleted:

Deleted: Same layout and format as the bottom panel (8-km level) of Figure 4.¶

Deleted: The vertical cross section of the of DAWN wind profiles sampling locations alongside the APR-2 nadir reflectivity profile is shown in Figure 10 (areas where the DC-8 was making a banking turn are omitted). Similar to flight segment 1, the two main "no-cloud" regions between APR-2 scans 600-900 and 1300-2000 are well sampled at the upper and lower heights levels. Near scan 850, DAWN data stops near 8-km in areas where APR-2 does not show any cloud, and several profiles near scan 900 sense deeper (to nearly 4-km), both of which may be from lidar backscatter off of clouds not sensed by APR-2 (i.e., below the minimum Ka-band detectability)[5]

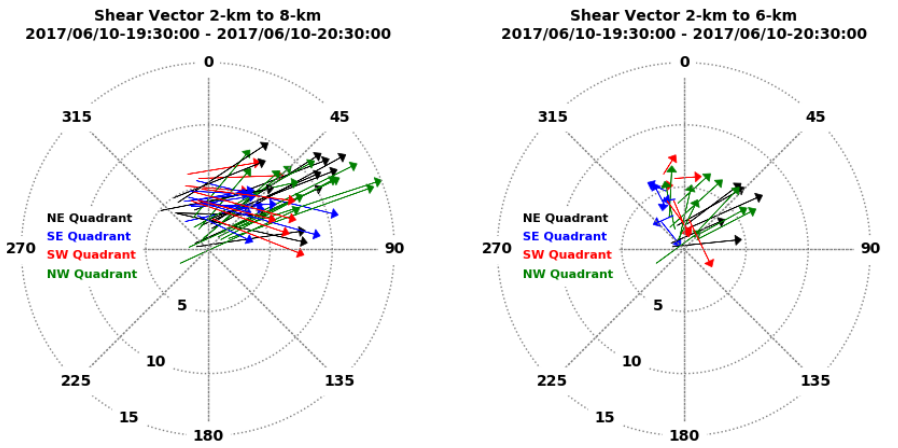

Figure 11. Same as Figure 7, but for flight segment 2 (1930-2030 UTC).

The vertical cross section of the DAWN wind profiles sampling locations alongside the APR-2 nadir reflectivity profile is shown in Figure 12 (areas where the DC-8 was making a banking turn are omitted). Similar to flight segment 1, the two main "no-cloud" regions between APR-2 scans 600-900 and 1300-2000 are well sampled at the upper and lower heights levels. Near scan 850, DAWN data stops near 8-km in areas where APR-2 does not show any cloud, and several profiles near scan 900 sense deeper (to nearly 4-km), both of which may be from lidar backscatter off of clouds not sensed by APR-2 (i.e., below the minimum Ka-band detectability). The lowest-most level retrieved by DAWN near scan 300 and again near scan 1200 appear to be the cloud top, which occurred in the 1.8-km blind zone (~ 8.2-10 km height) area where APR-2 does not provide any data. Near scan 400, there are numerous DAWN profiles provided in cloud gaps as the DC-8 passed through some higher-level clouds.

Formatted: Centered
Formatted Table
Formatted: Font: 9 pt, Bold
Formatted: Font: 9 pt, Bold
Formatted: Font: 9 pt, Bold

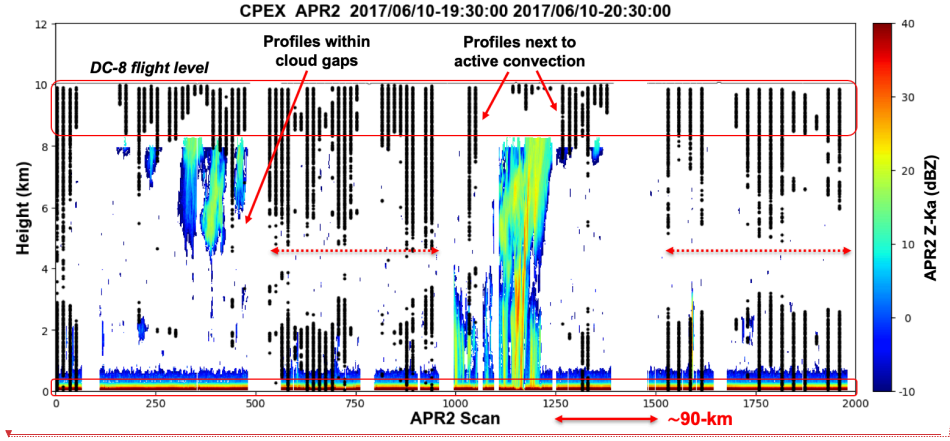

Figure 12. Cross-section of the APR-2 Ka-band reflectivity (color scale to right) during segment 2 (1930-2030 UTC). Same layout and format as Figure 8.

3.3 Flight Segment 3 (2030-2130 UTC).

Flight segment 3 begins with the DC-8 heading in a northerly direction. The flight revisited some of the area sampled during the previous segment by executing a box pattern in clockwise direction, before exiting to the east along a 90-degree bearing (Figure 13). Towards the end of this flight segment, the DC-8 dropped to a 9-km flight level. At 8-km height, 25 DAWN wind vectors were estimated from the LOS data processing.

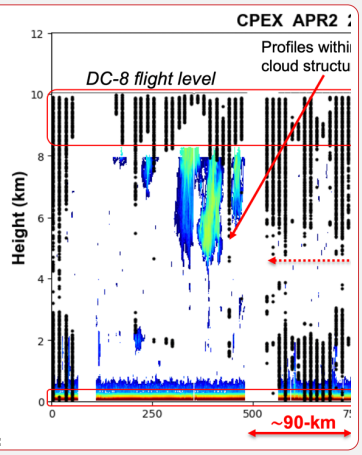

Deleted:

Deleted: 0

Deleted: S

Deleted: 7

Deleted: where flight segment 2 ended,

Deleted: 1

Deleted: (at 2-km, 18 DAWN vectors were available

Deleted:)

Deleted: The weak directional shear on the south and southwestern regions of the AOI is still present, with 8-km westerly winds and 2-km southerly winds (not shown) near 5 m s^{-1} speeds. On the north side of the AOI, 8-km winds are mostly southwesterly near 15 m s^{-1}. At the 2-km level, 18 DAWN wind vectors were estimated, nearly all concentrated on the south side of the AOI, but several southeasterly 5 m s^{-1} winds were estimated on the north side of the AOI. Figure 12 shows the DAWN vertical sampling density during this flight segment relative to the APR-2 Ka-band reflectivity structure. On the east and south sides of the AOI the DC-8 passed above a region of thin clouds (as shown in the IR background in Figure 11), but were not detected by (i.e, below the sensitivity of) APR-2 except for some 2-km cloud tops near scan 1100. Overall in this region, DAWN sampling was reduced in the 2-8 km height level, but the E-W leg (scans 1200-1400) provided profiling to the surface in many locations.

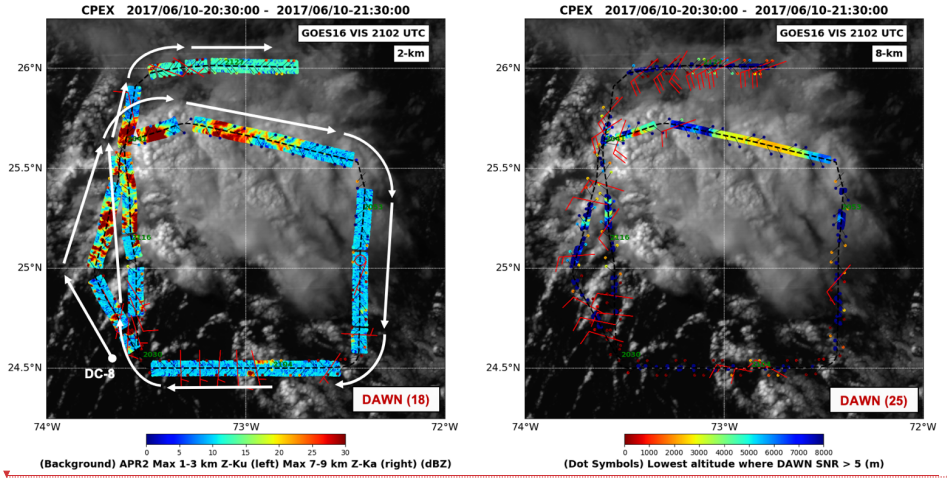

Figure 13. DC-8 flight line during segment 3 (2030-2130 UTC) on 10 June 2017. Same layout and format as Figure 10.

The 90-degree directional shear on the SW quadrant of the AOI is still present, measuring about 5 m s^{-1} in magnitude (Figure 14), but insufficient 8-km winds were obtained in the other quadrants for comparison (at the 2-km level, only 18 DAWN wind vectors were estimated, nearly all concentrated on the south side of the AOI).

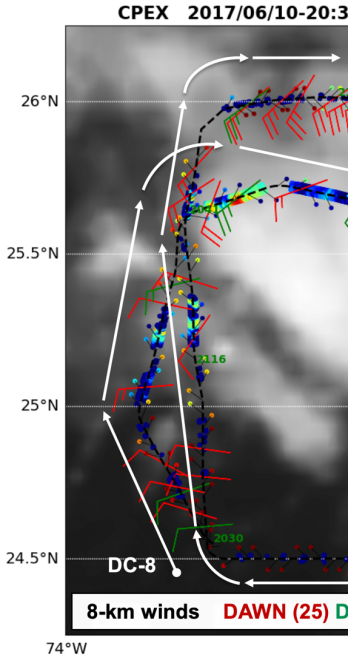

Deleted:

Deleted: 1

Deleted: S

Deleted: The GOES-East IR imagery at 2100 UTC is shown in the background grayscale (white=cold; black=warm). Same

Deleted: the bottom panel (8-km level) of

Deleted: 4

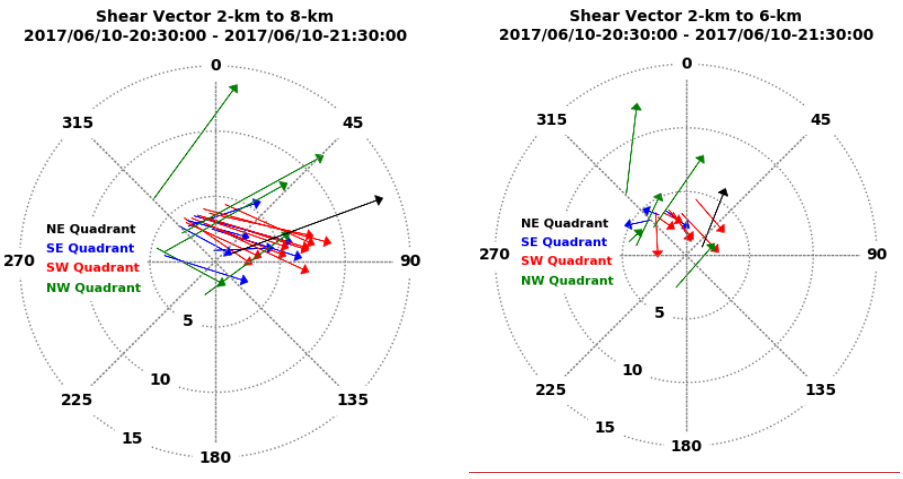

Figure 14. Same as Figure 5, but for flight segment 3 (2030-2130 UTC).

Figure 15 shows the DAWN vertical sampling density during this flight segment relative to the APR-2 Ka-band reflectivity structure. On the east side of the AOI the DC-8 passed above a region of thin clouds (as shown in the IR background in Figure 11), but were below the sensitivity of APR-2. This could be one reason for the reduced DAWN sampling between APR-2 scans 700-1000 in the 2-8 km height level, but the E-W leg (scans 1200-1400) provided DAWN profiling to the surface in many locations.

Formatted Table

Formatted: Normal

Formatted: Normal

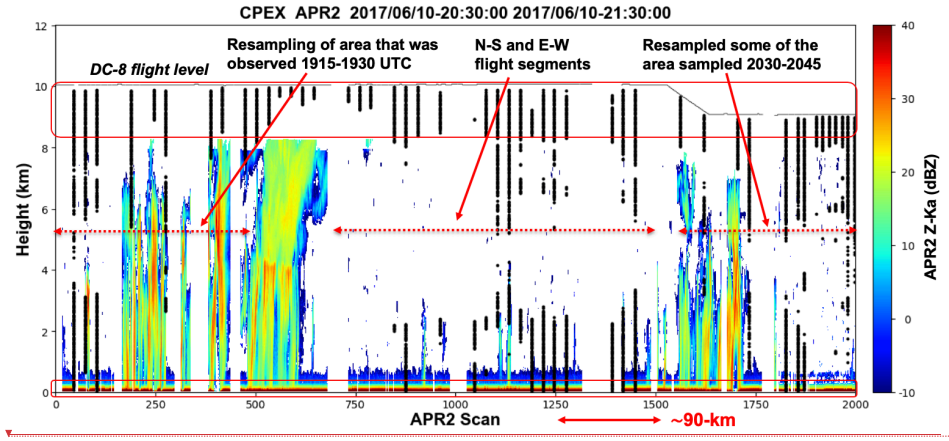

Figure 15. Cross-section of the APR-2 Ka-band reflectivity (color scale to right) during segment 3 (2030-2130 UTC). Same layout and format as Figure 8.

600

3.4 Flight Segment 4 (2130-2230 UTC).

Flight segment 4 begins with the DC-8 heading in an easterly direction and then banking to a 225-degree bearing. The DC-8 partially completed a figure-eight pattern, before exiting to the west along a 270-degree bearing and returning to Florida, as shown in Figure 16. The total DAWN profile sampling numbers are higher than segment 3, with 49 and 63 DAWN vectors
605 provided at 2- and 8-km heights, respectively. The cloud system near 25.5N 73.5W has matured considerably relative to its structure in previous flight segments, represented with a fairly well-defined melting level shown near scans 1450-1550.

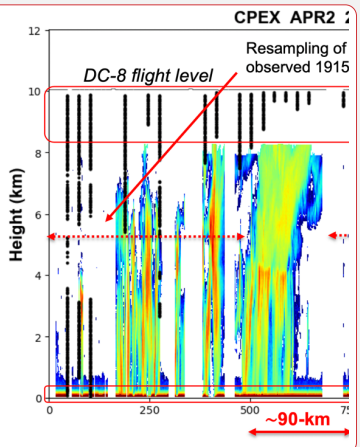

Deleted:

Deleted: 2

Deleted: S

Deleted:

Deleted: 7

Deleted: 3

Deleted: overall

Deleted: Small growing clouds were first overflown during scans 200-400. …

Deleted: with

Deleted: bright band

Deleted: DAWN vertical sampling density during this time is fairly dense (Figure 14), with more winds provided in the 2-6 km height level than during flight segment 3, notably in the middle and end of this flight segment. When the DC-8 moved to a lower 9-km flight level, the pulse width was changed resulting in the APR-2 blind zone being shorted by one-half (to 0.9 km), which is evident for the tallest clouds near scans 400 and 1400. DAWN also provided overall better sampling in the mid-levels from this lower flight altitude, with almost complete top-bottom profiles towards the end of the flight segment.¶ … [6]

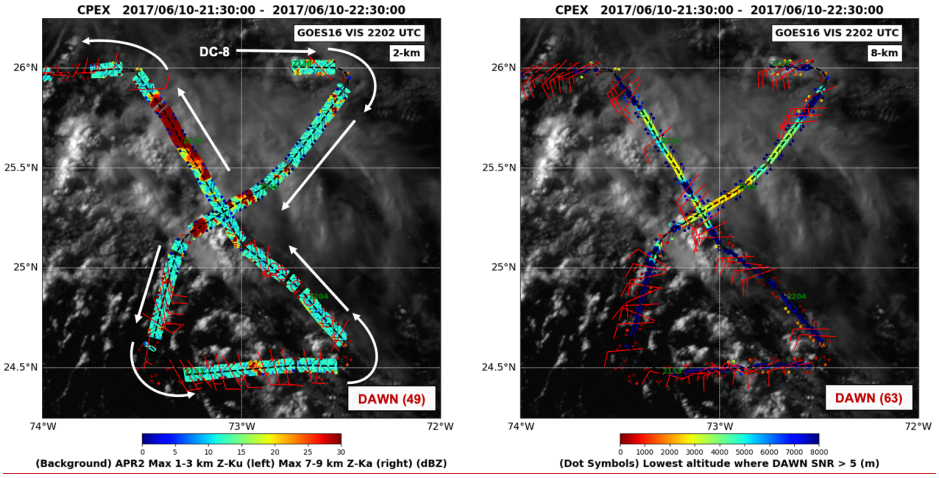

Figure 16. DC-8 flight line during segment 4 (2130-2230 UTC) on 10 June 2017. Same layout and format as Figure 10.

Deleted: 3

Deleted: S

Deleted: The GOES-East IR imagery at 2200 UTC is shown in the background grayscale (white=cold; black=warm). Same

Deleted: the bottom panel (8-km level) of

Deleted: 4

Figure 17 shows the shear in the NW quadrant between 2- and 8-km (and between 2-km and 6-km), pointing towards the northeast along a near-radial direction (little directional shear). This period also gathers sufficient DAWN data in the SE quadrant (blue vectors) that was not well sampled in the earlier time segments. This shows evidence of shear between 2-km and 6-km pointing to the north, but shear between 2-km and 8-km pointing towards the east.

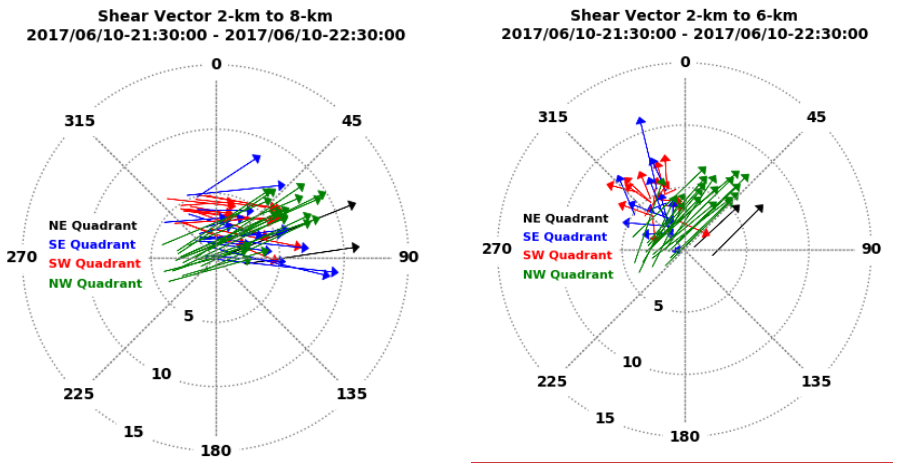

Figure 17. Same as Figure 5, but for flight segment 4 (2130-2230 UTC).

Narrow growing clouds were first overflown during scans 200-400 (Figure 18). DAWN vertical sampling density during this time is fairly dense, with more winds provided in the 2-6 km height level than during flight segment 3, notably in the middle and end of this flight segment. When the DC-8 moved to a lower 9-km flight level, the pulse width was changed resulting in the APR-2 blind zone being shorted by one-half (to 0.9 km), which is evident for the tallest clouds near scans 400 and 1400. DAWN also provided overall better sampling in the mid-levels from this lower flight altitude, with almost complete top-bottom profiles towards the end of the flight segment.

Formatted Table

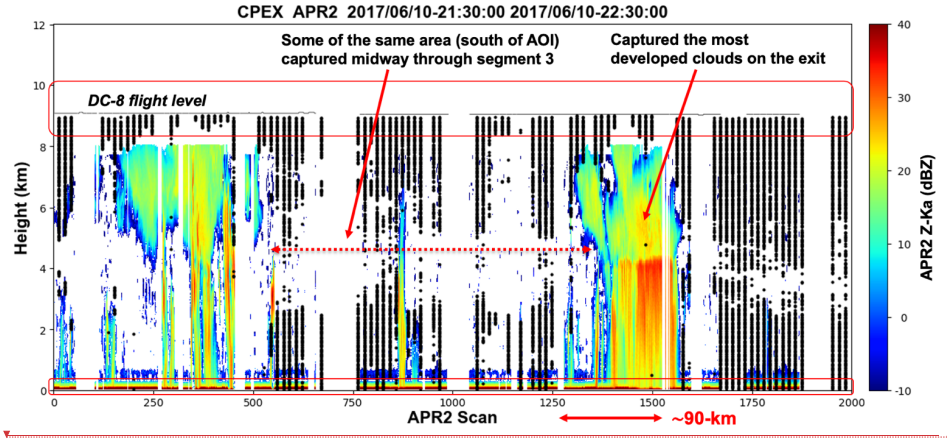

Figure 18. Cross-section of the APR-2 Ka-band reflectivity (color scale to right) during segment 4 (2130-2230 UTC). Same layout and format as Figure 8.

4 DAWN and APR-2 horizontal winds on 11 June 2017.

APR-2 also provided vertical air motion and structure of the cloud systems in the cloud-detected regions where the DAWN profiling capability was degraded. The purpose of this section is to examine a method to couple the two wind estimates near clouds. By viewing clouds from multiple viewing directions near nadir, airborne Doppler radars sample a mixture of the vertical and horizontal winds associated with the movement of the hydrometeors being sensed (*Heymsfield et. al.*, 1996). As the DC-8 moves forward and the APR-2 scans across-track, the measured Doppler velocity represents a combination of the vertical and across-track components of the hydrometeor motion within each APR-2 range bin (*Durden et. al.*, 2003). These data can provide some complementary wind direction information to complement DAWN, and under the right conditions (no significant horizontal shear across the APR-2 scan swath) provide some continuity in the wind measurements between the cloud and no-cloud areas. The received Doppler velocity represents contributions from the motion of the hydrometeors owing to air motion, and the contribution owing to the (reflectivity-weighted) hydrometeor fall speed. Define θ as the viewing angle from nadir (e.g., zero represents straight downward, and negative and positive denote the left and right sides of the APR-2 swath, respectively), and v_z and v_y as the vertical and across-track wind components. Then the Doppler wind at corresponding left and right sides of the swath is given by:

$$v_{left} = v_z cos|\theta| - v_y sin|\theta| \quad (1)$$

Deleted:
Deleted: 4
Deleted: S
Deleted:
Deleted: 7
Deleted: 's
Deleted: r

$$v_{right} = v_z cos|\theta| + v_y sin|\theta| \quad (2)$$

where the subscripts left and right refer to the corresponding APR-2 beam positions at $-\theta$ (left side of swath) and $+\theta$ (right side of swath), respectively. The vertical (z) and across-track (y) wind components are easily solved for,

$$v_z = (v_{right} + v_{left})/2cos|\theta| \quad (3)$$

$$v_y = (v_{right} - v_{left})/2sin|\theta| \quad (4)$$

Note that in this formulation, the effects owing to the hydrometeor fall speeds are still included, so the estimate of v_z in (3) is not the same as the vertical (w component) wind due to air motion only. To account for the fall speed, the fall speed-reflectively relation developed by Black et al. (1996) is applied and only the 8-km level winds (where there has not yet been significant attenuation) are assessed. After this correction, v_z is assumed equal to the w wind owing to air motion. However, in general more rigorous radar inversion methods that account for the radar attenuation and the hydrometeor Doppler fall speed are required before this formulation can be applied to lower cloud levels (*Guimond et. al.*, 2014)

This principle is examined on the APR-2 data gathered between 1800-2100 on 11 June 2017. Figure 19 shows the plan view, where there are abundant DAWN wind vectors at 8-km, including many that are close to clouds. There are six flight legs along a predominant 90-degree (W-E) or 270-degree (E-W) (+u and -u wind component direction, respectively) flight bearings, beginning near 1800, 1815, 1838, 1900, 1920 and 1955 UTC (with some slight deviations along these directions to avoid deep clouds near flight level). The first and last three of these flight legs occurred in predominantly cloud-free and cloud-covered conditions, respectively. The top panel of Figure 20 shows the time intervals corresponding to these 90- and 270-degree bearings. In these flight directions, the APR-2 across-track wind component v_y (4) is solely contributed by the v wind. When the DC-8 transitions from a 90- to 270-degree flight bearing (or vice-versa), a flip in the sign of the APR-2 v_y component is expected, since the APR-2 right swath side becomes the left swath side.

Deleted: 5

Deleted: of the 8-km level winds from DAWN

Deleted: providing

Deleted: abundant

Deleted: s

Deleted: some

Deleted: vectors

Deleted: , as shown by the APR-2 Ka-band reflectivity at this level. The DC-8 entered the area from the northeast.

Deleted: The DC-8 entered the area from the northeast.

Deleted: ,

Deleted: 16

Formatted: Font: Italic

Formatted: Font: Italic, Subscript

Formatted: Subscript

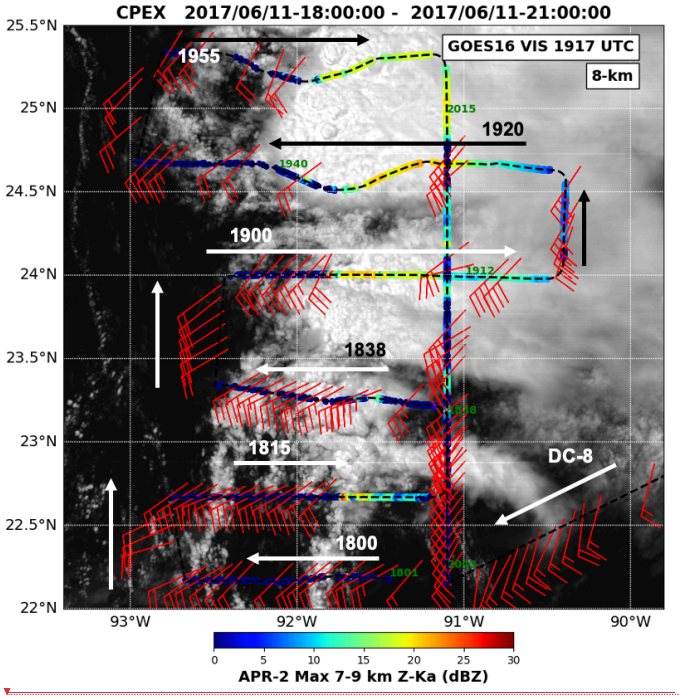

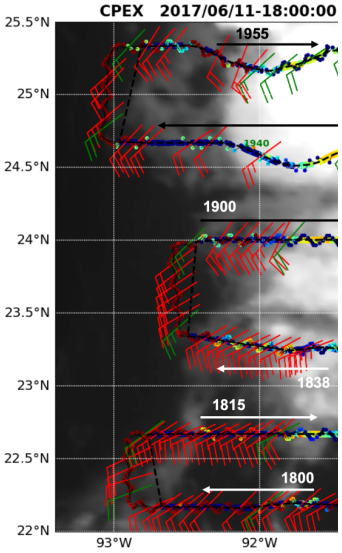

Figure 19. DC-8 flight lines during 1800-2130 UTC on 11 June. Same layout and format as Figure 4, but only for the 8-km level. The six E-W or W-E flight lines beginning near 1800, 1815, 1838, 1900, 1920 and 1955 UTC are shown.

735

The bottom panel of Figure 20 shows the APR-2 vertical (v_z) and across-track (v_x) winds estimated from (3) and (4), plotted in orange and black colors, respectively. DAWN (u, v) winds at the same 8-km level are shown in red and blue colors, respectively. Near 1830 UTC, the DAWN v component is near 5 m s^{-1}, and the APR-2 v component is near 5-10 m s^{-1}, but quickly (within a few minutes) changes to a smaller value as the DC-8 enters an area with stronger vertical motion and
740 assumptions on horizontal shear are likely voided. Near 1840 when the DC-8 is flying along a 270-degree bearing and detects clouds at the 8-km level, the APR-2 v component changes to -12 m s^{-1}. While it is the expected wind speed sign flip, it is more difficult to compare the wind speed magnitude. Also, the 270-degree bearing has some deviations near 1843 UTC to avoid convection at flight level.

Deleted:

Deleted: 5

Deleted: 2017. The GOES-East IR imagery at 1900 UTC is shown in the background grayscale (white=cold; black=warm).

Deleted: the bottom panel (8-km level) of

Deleted: 4

Deleted: 16

Deleted: w

Formatted: Subscript

Formatted: Subscript

Deleted: colors

Deleted: colors

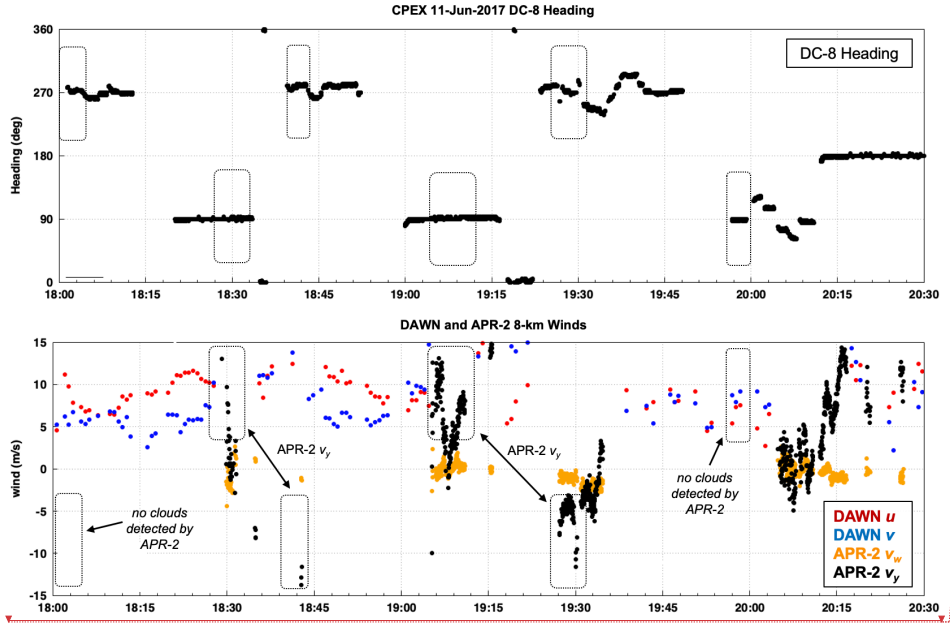

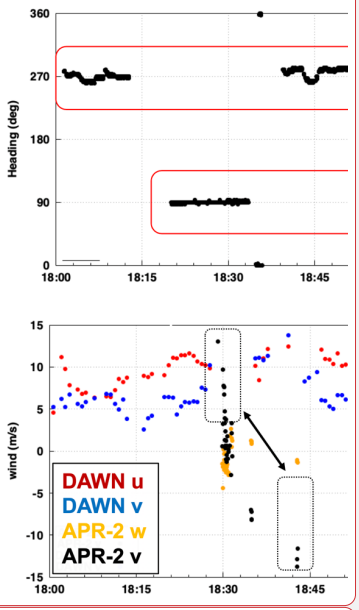

Figure 20. (Top) DC-8 heading between 1800-2130 UTC on 11 June 2017, highlighting the six time periods depicted in Figure 19. (Below) DAWN (*u*, *v*) wind vectors at the 8-km level (red and blue points, respectively). APR-2 (v_w, v_y) winds (orange and black, respectively) estimated from (3) and (4).

A second coincidence occurs between the APR-2 data near 1910 and 1925 UTC, where the APR-2 v_y component flips sign between similar wind speed values. However, the area at 1925 UTC is so cloud-filled that there are no nearby DAWN wind profile data to compare to. It also represents an area with stronger vertical winds, where the assumption of no significant horizontal shear across the APR-2 scan swath is likely not valid. While this is not a rigorous comparison of DAWN and Doppler precipitation radar horizontal winds, the principle could be applied to any these data from any close time pair of DC-8 flight bearing segments that are separated by 180-degrees. In this example, the flight bearings were fortuitously along easterly or westerly directions. For any arbitrary flight bearing, the cross-track winds estimated by (4) are more generally a combination of (*u, v*), and the DAWN (*u, v*) winds could be transformed to these same directions for comparison. This complement of Doppler radar and DWL observations could provide a means to link horizontal wind data outside of clouds

Deleted:
Deleted: ¶
Deleted: 16
Deleted: 5
Formatted: Subscript
Formatted: Subscript
Formatted: Font: Italic
Formatted: Font: Italic, Subscript
Formatted: Font: Italic
Deleted: DWL
Deleted: arbitrary
Deleted: T

and inside clouds (away from strong vertical motion, from APR-2), an important transition region. Space-based Doppler radar measurement methods to estimate the horizontal LOS (HLOS) wind in-cloud have been proposed (*Illingworth et. al*., 2018), as one means to complement the HLOS winds from Aeolus. However, further investigation from CPEX and other APR-2 airborne data are needed to assess the quality of the radar wind components before they can be used for science or model data assimilation purposes.

5 Conclusions.

This manuscript has presented joint observations from the DAWN Doppler wind lidar and the APR-2 (Ku/Ka-band) Doppler precipitation radar, collected during the CPEX campaign in 2017. Data from NASA DC-8 flight segments from two flight dates were examined to assess the ability of DAWN to sense air motion nearby to developing convection. The flight patterns on June 10-11 were selected for this purpose. For the June 10 flight date, the DC-8 arrived on-station to the area of interest, with sufficient time to capture the evolution of isolated, small-scale (< 10-km horizontal extent, many not yet glaciated) clouds from numerous DC-8 repeat passes for about a 3-hour period. The environment surrounding the clouds on this date exhibited directional shear between the 2- and 8-km levels in the quadrant SW of the developing convection. A number of growing convective clouds with APR-2 echo tops below 5-km were sampled by the APR-2, away from the more developed convection. The capability of DAWN to collect LOS profiles near convection was highlighted for several passes where profile retrievals were possible up to the edges of many APR-2 detected cloud systems. On June 11, the DC-8 sampling pattern consisted of successive repeat passes on E-W and W-E flight bearings, where the cross-track winds from APR-2 were examined for consistency with nearby DAWN winds, in the proximity of cloud edges.

As stated in the introduction, this manuscript provides the observational context for a separate mesoscale model data assimilation study, which is aimed at quantifying the impact of the DAWN measurements on the analyzed atmospheric state variables and on the forecasted precipitation when the DAWN wind profile observations were assimilated into the model (*Zhang et. al*., 2019). While only limited examples are shown, these particular findings highlight the importance of when and where the wind observations are taken, and provide guidance for assessing observational strategies and requirements needed for future airborne field campaigns with similar instrumentation.

Deleted: examine

Deleted: 3 hour

Deleted: relatively weak

Deleted: area south and southeast

Deleted: analyzed

Deleted: will

Deleted: aid

Deleted: in

Deleted: future

Deleted: and limitations on the scale (horizontal and vertical) of the observations …

Deleted:

Data Availability

The DAWN LOS and profile data (ASCII text format) and APR-2 data (HDF5 format) are available from the authors upon request.

Team list

Author Contribution

ST, SLD and OS carried out the APR-2 data pre-processing to produce Level-1 reflectivity products. FJT carried out the data alignment between DAWN and APR-2. All JPL authors contributed to operations of the APR-2 during CPEX. SG and GDE collected and performed all DAWN data processing.

Competing Interests

The authors declare that they have no conflict of interest.

Acknowledgements

The work contained in this presentation was carried out at the Jet Propulsion Laboratory, California Institute of Technology, under a contract with NASA. © 2020 all rights reserved. Support from NASA under the Weather and Atmospheric Dynamics program is recognized. The authors gratefully acknowledge the DC-8 flight support team, the CPEX Co-Investigators Ed Zipser and Shuyi Chen, and Kristopher Bedka (NASA Langley Research Center) for his assistance with GOES data processing.

References

Baker, W.E., Atlas, R., Cardinali, C., Clement, A., Emmitt, G.D., Gentry, B.M., Hardesty, R.M., Källén, E., Kavaya, M.J., Langland, R., Ma, Z., Masutani, M., McCarty, W., Pierce, R.B., Pu, Z., Riishojgaard, L.P., Ryan, J., Tucker, S., Weissmann, M., and Yoe, J.G.: Lidar-Measured Wind Profiles: The Missing Link in the Global Observing System. *Bull. Amer. Meteor. Soc.* ***95***, 543–564, https://doi.org/10.1175/BAMS-D-12-00164.1, 2014.

Black, M. L., Burpee, R. W., & Marks, F. D.: Vertical Motion Characteristics of Tropical Cyclones Determined with Airborne Doppler Radial Velocities. *Journal of the Atmospheric Sciences*, *53*(13), 1887–1909. https://doi.org/10.1175/1520-0469(1996)053<1887:VMCOTC>2.0.CO;2, 1996.

Black, P., Harrison, L., Beaubien, M., Bluth, R., Woods, R., Penny, A., Smith, R.W., and Doyle, J.D.: High-Definition Sounding System (HDSS) for Atmospheric Profiling. *J. Atmos. Oceanic Technol.,* **34**, 777–796, https://doi.org/10.1175/JTECH-D-14-00210.1, 2017.

Deleted: The work contained in this presentation was carried out at the Jet Propulsion Laboratory, California Institute of Technology, under a contract with NASA. © 2020 all rights reserved. Support from NASA under the Weather and Atmospheric Dynamics program is recognized. The authors gratefully acknowledge the DC-8 flight support team, and the CPEX Co-investigators Dr. Ed Zipser and Dr. Shuyi Chen.¶

Bucci, L. R., O'Handley, C., Emmitt, G. D., Zhang, J. A., Ryan, K., & Atlas, R.: Validation of an Airborne Doppler Wind Lidar in Tropical Cyclones. *Sensors (Basel, Switzerland)*, *18*(12), 4288. doi:10.3390/s18124288, 2018.

Chen, S.S., Kerns, B.W., Guy, N., Jorgensen, D.P., Delanoë, J., Viltard, N., Zappa, C.J., Judt, F., Lee, C.-Y., and Savarin, A.: Aircraft Observations of Dry Air, the ITCZ, Convective Cloud Systems, and Cold Pools in MJO during DYNAMO. Bull. Amer. Meteor. Soc. **97**, 405–423, doi.org/10.1175/BAMS-D-13-00196.1, 2015.

Durden, S.L., Tanelli, S., and Im, E., 2012. Recent observations of clouds and precipitation by the airborne precipitation radar 2nd generation in support of the GPM and ACE missions. Proc. SPIE 8523, Remote Sensing of the Atmosphere, Clouds, and Precipitation IV, International Society for Optics and Photonics, 85230M, https://doi.org/10.1117/12.977574, 2012.

Durden, S.L., Li, L., Im, E., and Yueh, S.H.: A Surface Reference Technique for Airborne Doppler Radar Measurements in Hurricanes. J. Atmos. Oceanic Technol. **20**, 269–275, doi.org/10.1175/1520-0426(2003)020<0269:ASRTFA>2.0.CO;2, 2003.

Flamant, P., Cuesta, J., Denneulin, M.-L., Dabas, A., and Huber, D.: ADM-Aeolus retrieval algorithms for aerosol and cloud products. *Tellus A: Dynamic Meteorology and Oceanography* ***60***, 273–286, 2008.

Guimond, S.R., Tian, L., Heymsfield, G.M., and Frasier, S.J.: Wind Retrieval Algorithms for the IWRAP and HIWRAP Airborne Doppler Radars with Applications to Hurricanes. J. Atmos. Oceanic Technol. 31, 1189–1215, doi.org/10.1175/JTECH-D-13-00140.1, 2014.

Heymsfield, G.M., Bidwell, S.W., Caylor, I.J., Ameen, S., Nicholson, S., Boncyk, W., Miller, L., Vandemark, D., Racette, P.E., and Dod, L.R.: The EDOP Radar System on the High-Altitude NASA ER-2 Aircraft. J. Atmos. Oceanic Technol. 13, 795–809, doi.org/ 10.1175/1520-0426(1996)013<0795:TERSOT>2.0.CO;2, 1996.

Horányi, A., Cardinali, C., Rennie, M. and Isaksen, L.: The assimilation of horizontal line-of-sight wind information into the ECMWF data assimilation and forecasting system. Part I: The assessment of wind impact. Q.J.R. Meteorol. Soc., 141: 1223-1232. doi:10.1002/qj.2430, 2015.

Hristova-Veleva, S., Knosp, B., Li, P.P., Vu, Q., Turk, F.J., Lambrigtsen, B., Su, H., Chen, S., and Zipser, E.J.: CPEX Data Portal: Status and Updates. *2nd CPEX Science Team Meeting*, 18-19 July, Univ. of Washington,

https://cpex.jpl.nasa.gov/scienceteammeeting/2019/SvetlaHristova-Veleva_Presentation1_CPEX_portals_2019_07_16_SHV_v02_final.pdf, 2019.

Illingworth, A.J., Battaglia, A., Bradford, J., Forsythe, M., Joe, P., Kollias, P., Lean, K., Lori, M., Mahfouf, J.-F., Melo, S., Midthassel, R., Munro, Y., Nicol, J., Potthast, R., Rennie, M., Stein, T.H.M., Tanelli, S., Tridon, F., Walden, C.J., and Wolde, M..: WIVERN: A New Satellite Concept to Provide Global In-Cloud Winds, Precipitation, and Cloud Properties. Bull. Amer. Meteor. Soc. 99, 1669–1687, doi.org/10.1175/BAMS-D-16-0047.1, 2018.

Jiang, H., Liu, C. and Zipser, E.J.: A TRMM-based Tropical Cyclone Cloud and Precipitation Feature Database. J. Appl. Meteor. Climatol., 50,1255-1274, doi.org/10.1175/2011JAMC2662.1, 2011.

Kavaya, M.J., Beyon, J.Y., Koch, G.J., Petros, M., Petzar, P.J., Singh, U.N., Trieu, B.C., and Yu, J.: The Doppler aerosol wind (DAWN) airborne, wind-profiling coherent-detection Lidar system: overview and preliminary flight results. Journal of Atmospheric and Oceanic Technology 31, 826–842, doi.org/10.1175/JTECH-D-12-00274.1, 2014.

Lux, O., Lemmerz, C., Weiler, F., Marksteiner, U., Witschas, B., Rahm, S., Schäfler, A., and Reitebuch, O.: Airborne wind lidar observations over the North Atlantic in 2016 for the pre-launch validation of the satellite mission Aeolus. *Atmospheric Measurement Techniques* ***11***, 3297–3322, doi.org/10.5194/amt-11-3297-2018, 2018.

Okamoto, K., Ishibashi, T., Ishii, S., Baron, P., Gamo, K., Tanaka, T.Y., Yamashita, K., and Kubota, T.: Feasibility Study for Future Space-Borne Coherent Doppler Wind Lidar, Part 3: Impact Assessment Using Sensitivity Observing System Simulation Experiments. *J. Meteorol. Soc. of Japan. Ser. II* ***96***, 179–199, doi.org/10.2151/jmsj.2018-024, 2018.

Pu, Z., Zhang, L., and Emmitt, G.D.: Impact of airborne Doppler Wind Lidar data on numerical simulation of a tropical cyclone , *Geophy. Res. Lett.*, **37**, L05801, doi:10.1029/2009GL041765, 2010.

Raymond, D., Fuchs, Ž., Gjorgjievska, S., Sessions, S.: Balanced dynamics and convection in the tropical troposphere. *Journal of Advances in Modeling Earth Systems* **7**, 1093–1116, https://doi.org/10.1002/2015MS000467, 2015.

Rowe, A.K., and Houze, R.A.: Microphysical characteristics of MJO convection over the Indian Ocean during DYNAMO. Journal of Geophysical Research: Atmospheres 119, 2543–2554, doi.org/10.1002/2013JD020799, 2014.

Rowe, A.K., Rutledge, S.A., and Lang, T.J.: Investigation of Microphysical Processes Occurring in Organized Convection during NAME. Mon. Wea. Rev. **140**, 2168–2187, doi.org/10.1175/MWR-D-11-00124.1, 2012.

Sadowy, G. A., Berkun, A.C., Chun, W., Im, E. and Durden, S.L., Development of an advanced airborne precipitation radar. *Microwave J.,* 46 (1), 84-98, 2003.

Šavli, M., Žagar, N., and Anderson, J.L.: Assimilation of horizontal line-of-sight winds with a mesoscale EnKF data assimilation system. *Q. J. Royal Meteorol. Soc, 144*, 2133–2155, doi.org/10.1002/qj.3323, 2018.

Schiro, K.A., and Neelin, J.D.: Deep Convective Organization, Moisture Vertical Structure, and Convective Transition Using Deep-Inflow Mixing. *J. Atmos. Sci*. *76*, 965–987, *doi.org/10.1175/JAS-D-18-0122.1*, 2019.

Stoffelen, A., Pailleux, J., Källén, E., Vaughan, J.M., Isaksen, L., Flamant, P., Wergen, W., Andersson, E., Schyberg, H., Culoma, A., Meynart, R., Endemann, M., and Ingmann, P.: The atmospheric dynamics mission for global wind field measurement. Bull. Amer. Meteor. Soc. **86**, 73–88, doi.org/10.1175/BAMS-86-1-73, 2005.

Tanelli, S., Durden, S.L., and Im, E.: Simultaneous measurements of Ku- and Ka-band sea surface cross-sections by an airborne radar. *IEEE Geosci. Remote Sens. Lett*., **3**, 359–363, 10.1109/LGRS.2006.872929, 2006.

Velden, C., Daniels, J., Stettner, D., Santek, D., Key, J., Dunion, J., Holmlund, K., Dengel, G., Bresky, W., and Menzel, P: Recent innovations in deriving tropospheric winds from meteorological satellites. Bull. Amer. Meteorol. Soc., 86, 205–224, doi.org/10.1175/BAMS-86-2-205, 2005.

Zhang, S., Hristova-Veleva, S., and Turk, F. J.: Assimilating the DAWN winds: Impact on the precipitation and flow structure of the June 10 squall line. *2nd CPEX Science Team Meeting*, 18-19 July, Univ. of Washington,. https://cpex.jpl.nasa.gov/scienceteammeeting/2019/SaraZhang_SvetlaHristoveVeleva_JoeTurk_20190717_CPEX_AssimilatingDAWN_June10_v05_final.pdf, 2019.

Zhang, J.A., Atlas, R., Emmitt, G.D., Bucci, L., Ryan, K.: Airborne Doppler Wind Lidar Observations of the Tropical Cyclone Boundary Layer. *Remote Sens*, *10*, 825, https://doi.org/10.3390/rs10060825, 2018.

Zipser, E.J., and M. Rajgopal.:L The June 10 case: Observations, satellite, DAWN, and dropsondes. *1st CPEX Science Team Meeting*, 7-8 June, Univ. of Utah, https://cpex.jpl.nasa.gov/scienceteammeeting/2018/Zipseretal.-%20forScienceTeamMeeting%20-V2.ppt, 2018.

Zipser, E.J., Twohy, C.H., Tsay, S.-C., Thornhill, K.L., Tanelli, S., Ross, R., Krishnamurti, T.N., Ji, Q., Jenkins, G., Ismail, S., Hsu, N. C., Hood, R., Heymsfield, G.M., Heymsfield, A., Halverson, J., Goodman, H.M., Ferrare, R., Dunion, J.P., Douglas, M., Cifelli, R., Chen, G., Browell, E.V., and Anderson, B.: The Saharan Air Layer and the Fate of African Easterly Waves—NASA's AMMA Field Study of Tropical Cyclogenesis. *Bull. Amer. Meteor. Soc.* ***90***, 1137–1156, doi.org/10.1175/2009BAMS2728.1, 2009.

Zuidema, P., Torri, G., Muller, C., and Chandra, A.: A Survey of Precipitation-Induced Atmospheric Cold Pools over Oceans and Their Interactions with the Larger-Scale Environment. *Surv. Geophys* ***38***, 1283–1305, https://doi.org/10.1007/s10712-017-9447-x 2017.

Page 8: [1] Deleted	Joe Turk	5/2/20 8:52:00 AM
Page 8: [1] Deleted	Joe Turk	5/2/20 8:52:00 AM
Page 8: [1] Deleted	Joe Turk	5/2/20 8:52:00 AM
Page 8: [1] Deleted	Joe Turk	5/2/20 8:52:00 AM
Page 8: [1] Deleted	Joe Turk	5/2/20 8:52:00 AM
Page 8: [1] Deleted	Joe Turk	5/2/20 8:52:00 AM
Page 8: [2] Deleted	Joe Turk	5/2/20 8:49:00 AM
Page 8: [3] Deleted	Joe Turk	5/2/20 8:49:00 AM
Page 8: [4] Deleted	Joe Turk	5/2/20 5:15:00 PM
Page 8: [4] Deleted	Joe Turk	5/2/20 5:15:00 PM
Page 8: [4] Deleted	Joe Turk	5/2/20 5:15:00 PM
Page 8: [4] Deleted	Joe Turk	5/2/20 5:15:00 PM
Page 8: [4] Deleted	Joe Turk	5/2/20 5:15:00 PM
Page 8: [4] Deleted	Joe Turk	5/2/20 5:15:00 PM
Page 16: [5] Deleted	Joe Turk	5/2/20 4:16:00 PM
Page 21: [6] Deleted	Joe Turk	5/2/20 4:59:00 PM